APN
ASIA-PACIFIC NETWORK FOR
GLOBAL CHANGE RESEARCH

FINAL REPORT

Transboundary transport of microplastics through atmospheric and oceanic currents in East Asia.

CRRP2019-FPO6-WANG

2024

Project Reference Number: CRRP2019-FP06-WANG

Project Duration: Nov 2020-Mar 2024

Funding Awarded:135000$

Grant DOI: https://doi.org/10.30852/p.13496

Date of Publication: 30 April 2024

Project Leader and Contact Details:

Lei Wang, college of Environmental Science and Engineering, Nankai University, China. Email: wang2007@nankai.edu.cn

Collaborators and Contact Details:

- Hongwen Sun, college of Environmental Science and Engineering, Nankai University, China. Email: sunhongwen@nankai.edu.cn
- Yuanyuan Dai, Bohai Fisheries Research Center, Chinese Academy of Fishery Sciences, China. Email: dai-yuanyuan2007@163.com
- Keisuke Kuroda, Department of Environmental and Civil Engineering, Toyama Prefectural University, Japan. Email: kuroda@pu-toyama.ac.jp
- Balt Suvdantsetseg, Department of International Cooperation and Correlation, Mongolian Academy of Sciences, Mongolia. Email: suvdantsetseg@mas.ac.mn

Recommended Citation:

Wang, L., Sun, H., Dai, Y., Kuroda, K., Suvdantsetseg, B. (2024). Transboundary transport of microplastics through atmospheric and oceanic currents in East Asia. Project Final Report. Asia-Pacific Network for Global Change research.

1. Summary

This study conducted observations during September, 2021 to August, 2023 in four East Asian cities, including Mandalgobi in south-central Mongolia, Hohhot and Tianjin in northern China, and Toyama on the west coast of Japan. By using Laser Direct Infrared imaging (LDIR) image system to detect microplastics (MPs) in suspended particulate matter and dust-fall, the distribution characteristics of AMPs in typical cities in East Asia were described, and the influence of meteorological factors on the distribution of AMPs was also explored. Based on the composition and aging characteristics of MPs, two methods were established to distinguish external MPs pollution. Using such methods, the risk of long-distance transport of AMPs in East Asia was evaluated under conventional weather conditions, as well as during dust events. In addition, this study calculated the radiative forcings of AMPs in different East Asian cities and compared the climate effects caused by AMPs.

Overall, both the concentration and the deposition flux of AMPs were positively correlated with the population density of sampling cities. In the coastal cities of Tianjin and Toyama, the distribution of AMPs was affected by wind direction, the AMPs concentration decreased when the wind blew from the ocean. Compared to that, the AMPs distribution of Mandalgobi was positively correlated by wind speed.

To establish reliable methods to distinguish external MPs, Siziwang banner (Size), a town on the Mongolian Plateau with a low population density and primarily engaged in pastoral activities, and Hohhot, an industrial city with much larger populations, were selected as targeted areas. Based on the sampling and detection results of the composition of MPs in outdoor dust, a composition-based Bray-Curtis similarity (Comp-BCs) index was established to evaluate the difference of composition between large and small sized (>25 μm and <25 μm) MPs. Besides, a carbonyl index-based BCs (CI-BCs) was established to evaluate the difference of aging characteristics between large and small sized MPs. Since small sized MPs have higher capacity for long-distance transport, and may undergo more severe environmental aging, both the lower Comp-BCs and the lower CI-BCs can serve as indicators of more input of external MPs.

By employing these two methods to evaluate the risk of long-distance transport of AMPs under normal weather condition, it was observed that the Comp-BCs and CI-BCs in the dust-fall of Mandalgobi were significantly lower than that in other cities. This indicates the presence of external MPs in Mandalgob. In addition, lower Comp-BCs and CI-BCs were also observed in the spring dust-fall of Hohhot, suggesting that Hohhot was significantly polluted by external small MPs during the spring season. During dust event, the Comp-BCs and CI-BCs of AMPs of Hohhot, Tianjin, and Toyama were all significantly lower compared to those on clean days, indicating the presence of external MPs pollution during the dust period. Backward trajectories show that the external small sized AMPs of Hohhot during spring and the dust even may have originated from the interior of Mongolian Plateau, while the external small sized AMPs of Toyama during the dust event may come from the East Asia continent.

Finally, it was found that the surface albedo has a great influence on the direction of the radiative forcing of AMPs, which lead to different climate effects caused by AMP in different East Asian cities. Tianjin showed the highest concentration of AMPs while with the lowest surface albedo, thus resulting in the smallest net radiative forcing at the top of the atmosphere (TOA) (-0.005±0.013 W/m^2). Compared to that, Mandalgobi showed the lowest AMPs concentration while with the highest surface albedo, resulting in a relative large net radiative forcing at TOA (0.022±0.006 W/m^2).

2. Objectives

– Objective 1: To describe the distribution characteristics of existing level, composition, and morphology of MPs in atmosphere (dust-fall and suspended particles) and ocean (water and sediments) in Japan, China and Mongolia. This is helpful to understand the environmental stock and potential environmental accumulation of plastic materials, and is significant for sustainable

– Objective 2: To confirm the existence of long-distance transport of MPs in East Asia and the influence of meteorological and hydrological factors. This will contribute to a better understanding of the contribution of climate change to the global transport of MPs, an important emerging pollutant.

– Objective 3: To assess the atmospheric and oceanic transport fluxes of MPs and to compare the contribution of local and foreign inputs. This will provide an important basis for the establishment of relevant international conventions and the formulation of MPs environmental management policies in the future.

3. Outputs, Outcomes and Impacts

Outputs	Outcomes	Impacts
A total of 7 suspended particulate samples were collected in Mandalgobi, Mongolia, from Jan 2022 to Jun 2022, and again in Jul 2023.	**The distribution of atmospheric microplastics in East Asian cities was described, along with an exploration of how meteorological factors affect this distribution.**	**Improved understanding of the environmental stock and potential accumulation of plastic materials in East Asia.**
A total of 24 suspended particulate samples were collected in Tianjin,	**Based on the composition and aging characteristics of MPs with different sizes, two methods were**	**Improved understanding of the risk associated with long-distance transport of atmospheric microplastic**

China, during Sep 2021 to Aug 2022.	**established to evaluate the contribution of external microplastics.**	**in East Asia.**
A total of 24 suspended particulate samples were collected in Toyama, Japan, from Sep 2021 to Aug 2022.	**The risks of atmospheric microplastics being transported from the interior of the Mongolian Plateau to North China under normal weather conditions and during a dust event were evaluated.**	**A scientific basis for intergovernmental collaboration in developing policies to control microplastic pollution.**
A total of 4 dust-fall samples were collected seasonally in Mandalgobi, Mongolia, from Sep 2021 to May 2022, and from Jun 2023 to Aug 2023.	**The risk of atmospheric microplastics being transported from the East Asian continent to the west coast of Japan during a dust event was assessed.**	**Improved understanding of the risk of climate changes caused by atmospheric microplastics in East Aisa.**
A total of 4 dust-fall samples were collected seasonally in Tian, China, during Sep 2021 to Aug 2022.	**Radiative forcing of atmospheric microplastics of typical cities in East Asia were calculated.**	
A total of 4 dust-fall samples were collected seasonally in Toyama, Japan, from Sep 2021 to Aug 2022.		
A total of 20 outdoor dust samples were collected in Siziwang banner and Hohhot, China, respectively, in Sep 2021.		
A suspended		

particulate sample during a dust event was collected on Apr 10th in Hohhot, China.		
A suspended particulate sample during a dust event was collected on Apr 10th in Tianjin, China.		
A suspended particulate sample during a dust event was collected on Apr 12th in Toyama, Japan.		

4. Key facts/Figures

- The monthly AMPs concentrationS of Mandalgobi, Tianjin and Toyama were 150.0±26.9 n/m^3, 335.1±69.2 n/m^3 and 217.8±54.1 n/m^3, respectively.
- The quarterly deposition fluxes of AMPs of Mandalgobi, Hohhot, Tianjin and Toyama were 4667±1995 n/m^3, 21131±4551 n/m^3, 25052±3533 n/m^3 and 5445±415 n/m^3, respectively.
- The distribution of AMPs of coastal cities (Tianjin and Toyama) in East Asia was significantly affected ($p<0.05$) by the wind direction, as lower concentrations and deposition fluxes were observed when the wind frequently blew from the ocean.
- Two methods to evaluate the contribution of external MPs were established, based on the composition and aging characteristics of MPs, respectively.
- There is a high risk of AMPs being transported from the interior of the Mongolian Plateau to North Chia during spring and dust events.
- There is a high risk of AMPs being transported from the East Asian continent to the west coast of Japan during dust events.
- The surface albedo has a great influence on the direction radiative forcing (DRF) of AMPs, which determine the climate effects caused by AMPs.
- AMPs tent to cause climate cooling for ocean, forest and snow field, while cause climate warming for grass land and bare soil.
- During the first half of 2022, the net DRFs of AMPs at the top of atmosphere (TOA) were 0.022±0.006 W/m^2, -0.005±0.013 W/m^2 and 0.013±0.029 W/m^2 in Mandalgobi, Tianjin and Toyama.

- Due to higher surface albedos in Mandalgobi and Toyama, the net DRFs of AMPs were positive during the first half of 2022, suggesting that AMPs caused climate warming in these two cities. In Tianjin, where the surface albedo is lower, a small net DRF of AMPs at TOA indicates a weak climate effect caused by AMPs.

5. Publications

1. An article has been submitted to ***Nature***, which is waiting for revision.

manuscriptrackingsystem nature

tracking system home | submission guidelines | reviewer instructions | help | logout | journal home

Detailed Status Information

Manuscript #	2024-02-02501
Current Revision #	0
Submission Date	5th February 24
Current Stage	Waiting for revision
Title	Leaf absorption is an important route of atmospheric microplastics to enter food chain
Manuscript Type	Biological Sciences - Article
Collection	N/A
Manuscript Comment	We suggest the following experts as potential reviewers for the manuscript. 1.Shuguang Wang, Shandong University, e-mail: wsg@sdu.edu.cn 2.Yongming Luo, Yantai Institute of Coastal Zone Research, Chinese Academy of Sciences, email: ymluo@issac.ac.cn 3.Jason C. White, Connecticut Agricultural Experiment Station, email: Jason.White@ct.gov 4.Xianzheng Yuan, Shandong University, email: xzyuan@sdu.edu.cn 5.Rong Ji, Nanjing University, email: ji@nju.edu.cn 6.Jian Zhao, Ocean University of China, e-mail: jzhao@ouc.edu.cn
Corresponding Author	Lei Wang (Nankai University)

2. An article has been submitted to ***ECO-Environment & Health***, which is under review.

Action	Manuscript Number	Title	Initial Date Submitted	Status Date	Current Status
View Submission Author Status Correspondence Publishing Options Send E-mail	EEHL-D-24-00150	Influence of regional environmental variables on the radiative forcing of atmospheric microplastics	Apr 18, 2024	Apr 26, 2024	Under Review

3 An article has been submitted to ***Environmental science and Ecotechnology***

Action	Manuscript Number	Title	Initial Date Submitted	Status Date	Current Status
View Submission Author Status Correspondence Publishing Options Send E-mail	ESE-D-24-00337	How to assess the external microplastics in areas with low human activities: A methodology based on polymer composition and aging degree	May 05, 2024	May 05, 2024	Manuscript Submitted

4. An article entitled " Mass distribution of PET and PC microplastics in the atmosphere of Tianjin, China " has been submitted to ***APN Science Bulletin***.

6. Media reports, videos and other digital content

List and hyperlink all resources and/or attach them to the present report for dissemination on the APN website.

- Introduction and operating videos to LDIR. (https://www.agilent.com.cn/zh-cn/product/molecular-spectroscopy/ldir-chemical-imaging-spectroscopy/ldir-chemical-imaging-system/ldir-chemical-imaging-system#videos)
- Realtime forecast for distributions of Asian dust and anthropogenic aerosols in east Asian region. (Forecast for distributions of Asian dust and anthropogenic aerosols in east Asian region (nies.go.jp)
- The website of AERONET, including aerosol optical parameters and environmental variables which can affect the radiative forcing of aerosols. Aerosol Robotic Network (AERONET) Homepage (nasa.gov)
- The website of NOAA Air Resources Laboratory enables online analysis of backward trajectories READY - (noaa.gov).
- The website of Omicshare enables online principal coordinates analysis (PCoA) (https://www.omicshare.com/tools/Home/Soft/pcoa).
- Optical parameters of MPs reported by Revell et al. (Direct radiative effects of airborne microplastics | Nature)

7. Pull quotes

Include up to three quotes from individuals (the head of your organisation, the project leader, a member of the research team, a local trainee, etc.) to demonstrate your project's impacts

- "I am very grateful for the opportunity to participate in the APN scientific research project. Under the leadership of Professor Lei Wang, we have conducted long-term observations on the concentration and deposition flux of atmospheric microplastics in several typical East Asian cities. I believe the results will help to enhance the public's understanding of the status of atmospheric microplastics pollution in East Asia".

Quated by Mr. Hanling Yang, a doctoral student of the research team from Nankai University, China.

- "I am honored to be involved in this APN project. I never thought that microplastics in the atmosphere could have an impact on the climate. Considering the huge production of plastic products in the world, the concentration of microplastics in the atmosphere is likely to increase over time, and the climate effects caused by them will certainly receive more attention."

Quated by Mr. Yining Xue, a doctoral student of the research team from Nankai University, China.

- "Microplastics is a completely new field for me. By participating in the APN project, I collected atmospheric particulates and dust-fall for the first time and learned the pre-treatment process of microplastics, which sparked my interest in studies related to microplastics. I believe this research is important because the distribution of microplastics in the atmosphere of Japan has not been reported before."

Quated by Ms. Yue Zhong, a master student of the research team from Toyama University, Japan.

8. Acknowledgments

The project team would like to acknowledge the services and contributions of all the team members from China, Mongolia and Japan. We thank the Nankai University, the Mongolian Academy of Sciences, and the Toyama Prefectural University for their support of this project, which includes, but is not limited to, providing observation sites and facilitating research work related to the APN project during the COVID-19 period

We are grateful to the Research Fellow Changsheng Guo at the Chinese Academy of Environmental Sciences, Associate Professor Wenyan Zhao at the Inner Mongolia University, and Dr. Fengmei Cao at China Agricultural University for their supports on sample collection, and we thank Dr. Jian Pu for her guidance on our APN work.

We are grateful to the Asia-Pacific Network for Global Change Research (APN) for its financial support We sincerely thank the APN team, including Ms. Nafesa Ismail, as well as other members, for their services and contributions.

9. Appendices

Provide a list of all appendices and attach them as separate files to the report.

1. The online launch meeting for the APN project was initiated by the research team from Nankai University, China in Dec, 2020.

2.

3. Associate Professor Keisuke Kuroda, the collaborator from Toyama Prefectural University, Japan, was invited by Nankai University to give an online lecture on groundwater pollution on November 6, 2021. Dr. Balt, the collaborator from Mongolian Academy of Sciences, Mongolia, was invited by Nankai University to give an online lecture on climate change caused by pastoral industry on November 20, 2021

4. Members of the Mongolian (left) and Japanese (right) research teams were cleaning glass cylinders used for collecting dust-fall samples. The cylinders, which adopt Chinese national standards, were sent from China to foreign countries for use in our project.

5. Members of the Chinese research team were conducting the LDIR detection.

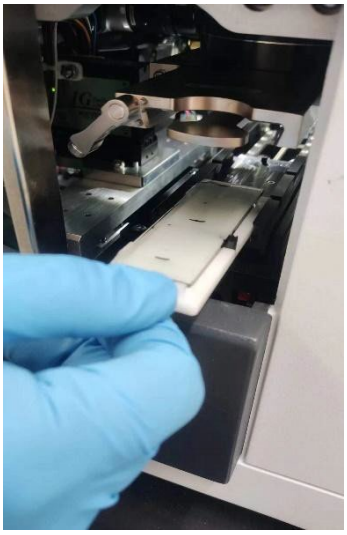

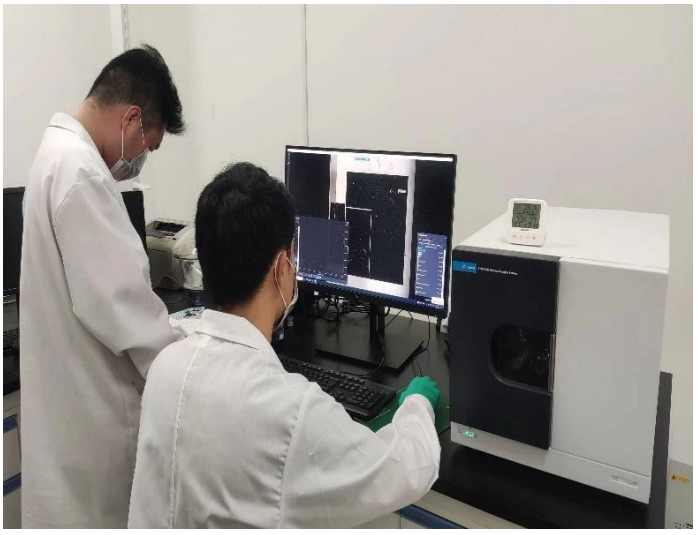

5 A detailed technical report (**on the next page Technical Report**)

Technical Report

CRRP2019-FP06-WANG

Abbreviated guidance

Abbreviation	Full name
MPs	Microplastics
AMPs	Atmospheric microplastics
LDIR	Laser infrared imaging
BCs	Bray-Curtis similarity
CI	Carbonyl index
PA	Polyamide
PC	Polycarbonate
PE	Polyethylene
PET	Polyethylene terephthalate
PP	Polypropylene
DRF	Direct radiative forcing
TOA	Top of the atmosphere
ES	Earth's surface
DRF_{SW}	DRF at short-wave band
DRF_{LW}	DRF at long-wave band
RAD_{SW}	Short-wave radiation
RAD_{LW}	Long-wave radiation

Table content

1 Introduction

Since the transport of MPs in the atmosphere is not limited by environmental boundaries, atmospheric transport may lead to wide diffusion of MPs[1]. MPs in the air may be transported by wind and deposited into the aquatic environment and the terrestrial environment, becoming a source of pollution to the terrestrial and aquatic ecosystems[2, 3]. Meanwhile, MPs deposited on the surface of the terrestrial environment may be re-transported into the air, forming a dynamic cycle among the air, terrestrial and aquatic ecosystems[4].

Although MPs have been widely detected in the atmosphere particulate matter and atmospheric dust-fall around the world[5-10], long-term observations of atmospheric MPs (AMPs) concentrations and AMPs deposition fluxes are still lacking in East Asia, which is one of the most densely populated regions in the world. Therefore, a better understanding of the spatial and temporal distribution characteristics of AMPs in East Asia is desperately needed.

In winter and spring, northwest winds prevail in Est Asia provide a natural channel for long-distance transport of atmospheric pollutants. For example, under the influence of the Mongolian cyclone, dust from southern and northwestern Mongolia can be transported to Japan and Korea [11-13]. In addition, black carbon can also be transported to Japan in a short period of time by dust storms in East Asia[14]. Theoretically, the transport dynamics of AMPs may be different with other aerosols due to the larger size of AMPs. However, considering the widely presence of MPs in the atmosphere all over the world, AMPs are likely to be transported though atmosphere under the control of East Asian monsoon and East Asia dust. However, due to the lack of reliable traceability methods, the risk of long-distance transport of AMPs in East Asia has not been evaluated yet.

In addition, plastics can absorb and scatter radiation[15-18], thus resulting in corresponding climatic effects, which can be quantified by the radiative forcing of AMPs. The net radiative forcing of aerosols can be obtained by adding the radiative forcing of long-wave and short-wave bands. The net radiative forcing at top of atmosphere (TOA) can be used to assess the climate effect caused by AMPs. The global average AMPs radiative forcing at TOA was -0.036 to 0.044 W/m^2, which was calculated based on the AMPs concentration of 100 n/m^3[19]. However, the radiative forcing of AMPs in East Asia has not been reported.

From 2021 to 2023, we collected suspended particulate samples and dust-all samples in four typical cities in East Asia. Using LDIR to detect MPs in the samples, the spatial and temporal distribution of AMPs in East Asia was described, and the factors affecting the distribution of AMPs was also explored. In addition, based on differences in composition and aging characteristics of MPs with different sizes, two methods for assessing the contribution of external MPs were established. Using these methods, the risk of long-distance transport of AMPs in East Asia under conventional weather conditions and during the dust event was evaluated, respectively. Finally, the annual radiative forcing of AMPs of Tianjin, and the influence of environmental variables on AMPs radiative forcing were evaluated. Furthermore, the climate effects caused by AMPs in three typical cities in East Asia cities during the first half of 2022 were compared.

2 The distribution of AMPs in East Asia

2.1 Methods

2.1.1 Researching area

Under the influence of the Mongolian and Siberian high, northwest winds prevail in winter and spring in the East Asian mainland, resulting in an atmospheric channel for the transport of pollutants from southeast to northwest[14]. To explore the long-distance transport process of AMPs in East Asia, four cities, including Mandalgobi of Mongolia, Hohhot and Tianjin of China, and Toyama of Japan were selected as targeted areas in this study (Fig 2.1). The geographical locations of such four cities were arranged from northwest to southeast (Fig 2.1), which was conducive to observe the long-distance transport of AMPs during the East Asian monsoon and East Asia dust period.

Mandalgobi (106.26E, 45.74N) is located in the south-central Mongolian Plateau (Figure 2.1) and is the capital of Mongolia's Central Gobi province. Mandalgobi is about 380 kilometers away from the border of China and Mongolia, and there is a possibility that air pollutants there can be transported downstream to China when the northwest wind prevails.

Hohhot (111.67E, 40.76N) is the capital of the Inner Mongolia Autonomous Region. Between Hohhot and the China-Mongolia border lies a vast expanse of grassland and desert with no discernible sources of MPs pollution, creating a favorable condition for observing the transport of AMPs from the interior of the Mongolian Plateau to North China.

Tianjin (117.34E, 38.99N), adjacent to the Bohai Sea (Fig 2.1), is one of the megacities in North China and also the closest city to Japan in North China. As a coastal city, Tianjin is located on the transport channel of air pollutants from East Asia mainland to the northwest Pacific Ocean, which makes it conducive to observe the transport of AMPs from East Asia mainland to Japan.

Toyama (137.10E, 36.71N) is located on the west coast of Japan, surrounded by mountains on three sides and with the Sea of Japan locating on the northwest (Figure 2.1). Due to its geographical location, Toyama may be less polluted by the surrounding cities, making it suitable for researching air pollutants transported across the sea from the East Asian mainland.

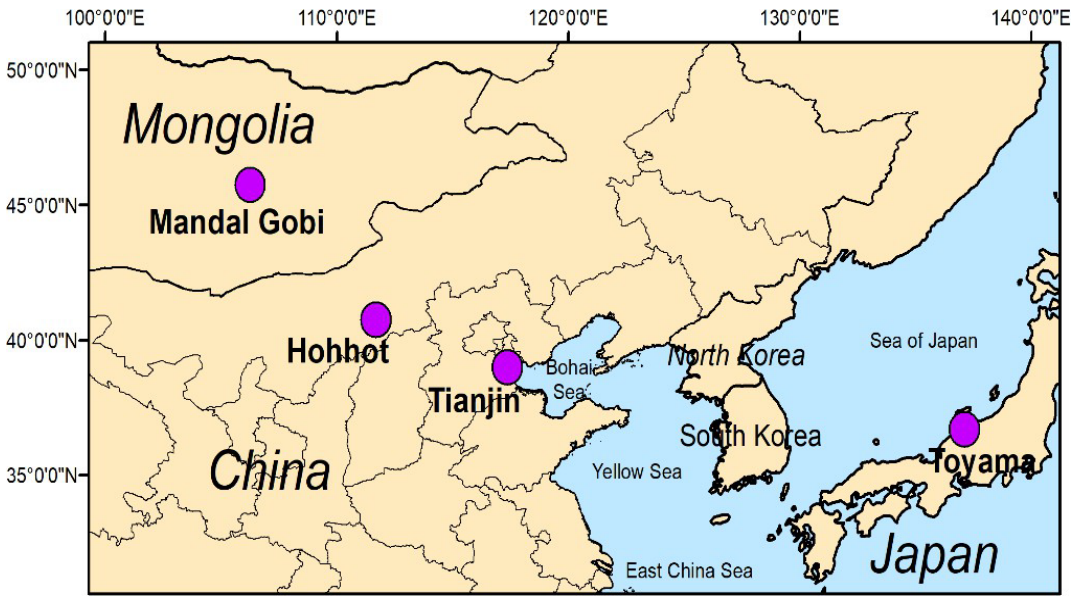

Figure 2.1 Dust-fall and suspended particulate matter sampling sites in four typical cities in East Asia (indicated by purple dots).

2.1.2 Sample collection

Dust-fall samples were collected quarterly in Hohhot, Tianjin, and Toyama from September 2021 to August 2022 (Fig 2.1). The sample collection in Mandalgobi was conducted from August 2021 to May 2022, with a suspension due to the impact of the COVID-19 pandemic. Thereafter, a supplemental summer dust-fall sample was collected from June to August 2023. The passive sampler which was used to collect dust-fall is consistent with three glass cylinders (inner diameter is 15 cm, height is 30 cm) and an iron bracket (Fig 2.2 A to D).

Atmospheric particulate samples were collected twice a month from September 2021 to August 2022 in Tianjin and Toyama by a middle flow (100 L/min) active sampler (Fig 2.1 E). The sample collection was conducted once a month from January to June 2021 in Mandalgobi by a high flow active sampler (Fig 2.1 F), and a supplemental sample was collected on July 2023.

A sandstorm forecast showed that two sandstorms appeared over the East Asia continent on the evening of April 10, 2023, one of which invaded North China, while the other passed through the northeast of China and continued to move eastward towards Japan (Fig 2.3 A). According to the forecast, atmospheric particulate samples were collected in Hohhot (Fig 2.3 B to C) and Tianjin on April 10, 2023, and collected in Toyama on April 12, 2023. The concentration of PM_{10} can serve as an indicator for the arrive of sandstorms[14]. Peak concentrations of PM_{10} were observed in all three sampling sites (Fig 2.3 D to F), indicating that suspended particulate samples during dust events were collected successfully in all three cities.

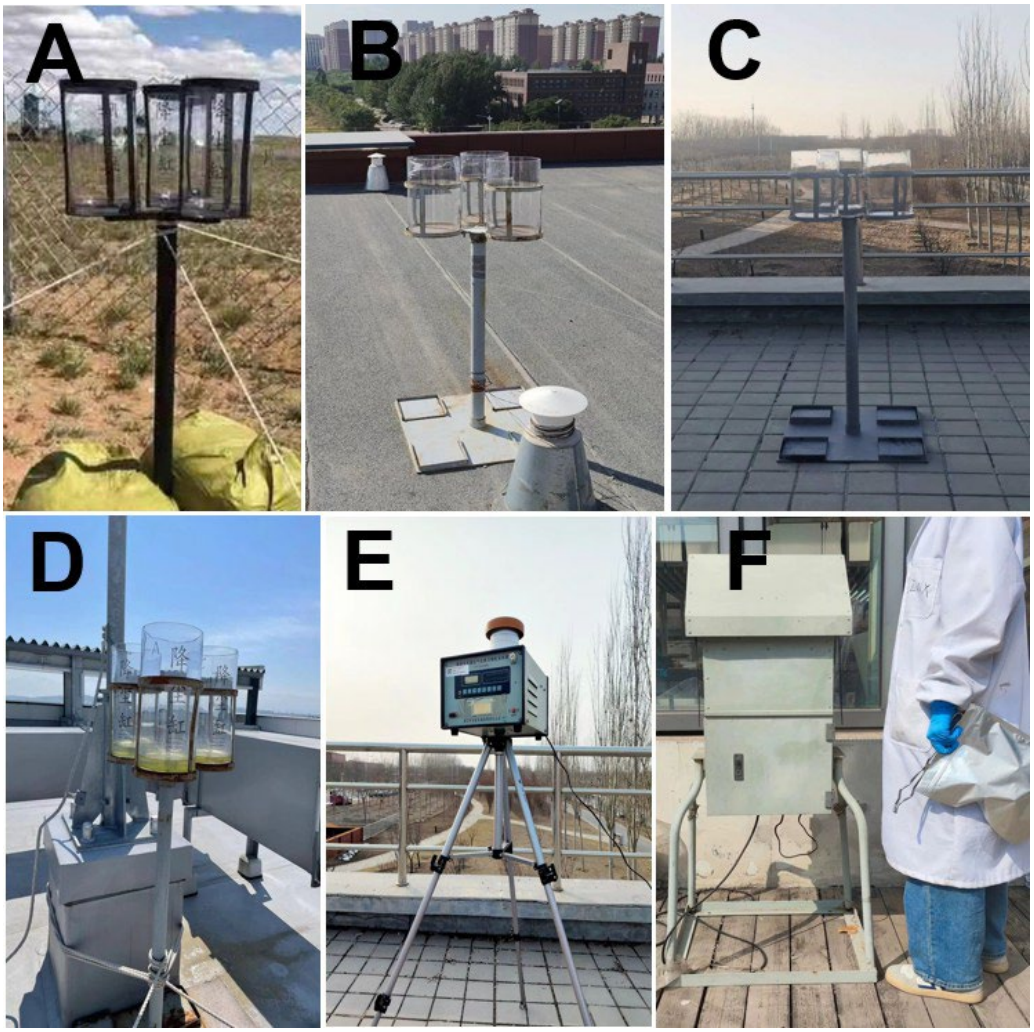

Figure 2.2 Passive samplers used to collect dust-fall in Mandalgobi (A), Hohhot (B), Tianjin (C) and Toyama (D). Medium flow (E) and high flow (F) active samplers which were used to collect suspended particulate samples.

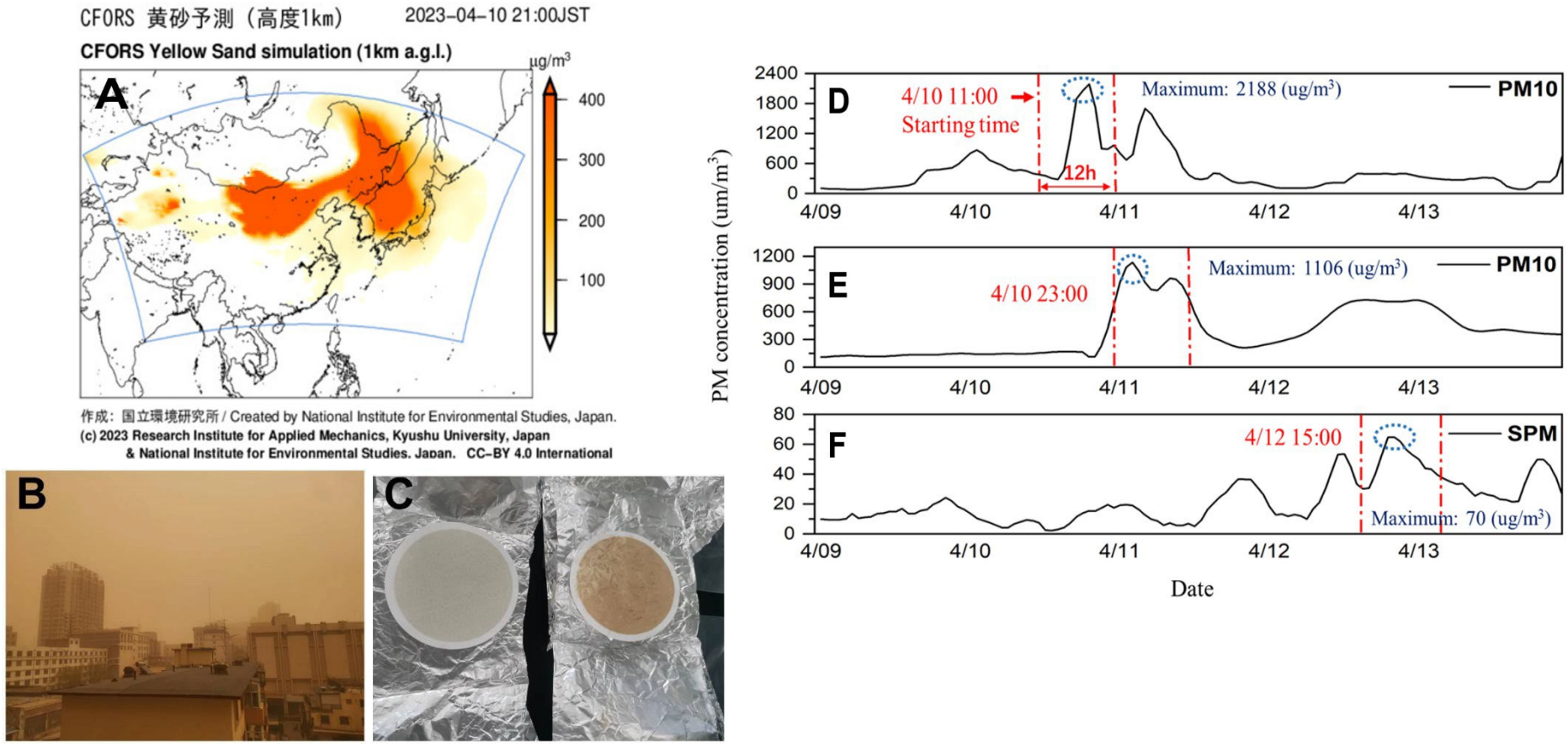

Fig 2.3 The distribution of dust concentration in East Asia at Beijing time 20:00 (A) (http://www-cfors.nies.go.jp/~cfors). The view of a dust event in Hohhot (B) and the comparison of suspended particulate samples collected on clean a day and during a dust event (C). The PM_{10} concentrations of Hohhot (D) and Tianjin (E) (https://www.mee.gov.cn), and the SPM concentration of Toyama (https://www.mee.gov.cn/) (F) during dust events. The concentration of suspended particulate matter (SPM), which is equal to about PM7, is an unique unit of Japan.

2.1.3 Pre-treatment of samples

For suspended particulate samples, filter membranes were carefully placed into clean aluminum foil after sampling, and transferred to the laboratory immediately. Each filter membrane was subjected to ultrasonic oscillation to separate the collected particles. AMPs in the collected particles were digested by 30% H_2O_2 and then floated by 52% $ZnCl_2$ solution. After the flotation process, the upper layer of $ZnCl_2$ solution was filtered through a mental filer with a pore size of 10 μm. Then, the mental filter was transferred into a 200 mL glass beaker with 20 mL of HPLC-grade ethanol and sonicated at 40000 Hz for 30 min. Then, the mental filter was removed by stainless steel tweezers, and the ethanol solution was concentrated into 1 mL by nitrogen. The concentrated solution was dropped on a high reflection glass window for LDIR detection after the ethanol volatilized.

The collected dust-fall was brushed off the wall of the cylinder using a hog hair brush firstly. Then, 100 mL of ultrapure water was added into the cylinder followed by placing the cylinder in an ultrasonic oscillator and ultrasonicating at a frequency of 40,000 Hz for 15 minutes. After ultrasonication, the cylinder was shaken to ensure no dust was left adhering to the walls. The washing solution was then filtered by a 2 mm metal sieve and transferred into a 1000 mL beaker. An additional 100 mL of ultrapure water was used to rinse the cylinder, and the washing solution was also transferred to the beaker. The beaker was then dried in an oven set at 70°C, with the cylinder being shaken every 12 hours to prevent dust from sticking to the walls.

After drying, the dust was scraped out with a stainless steel spoon. Then, 0.02 g of the dust-fall was placed in a high-type beaker and 20 mL of H_2O_2 (30%) was added to digest the dust sample. The beaker was placed in a 70°C water bath until the solution was clear and no longer bubbling. After evaporating the H_2O_2, 100 mL of $ZnCl_2$ solution (52%) was added, and after standing for 12 hours, 30 mL of the supernatant was passed through a metal filter membrane with a 10 μm pore. The filter membrane was then placed in a 200 mL beaker with the addition of 15 mL of ethanol, and the mixture was ultrasonicated at 40,000 Hz frequency for 30 minutes. After ultrasonication, the filter membrane was removed by a stainless steel tweezer, and the ethanol solution was concentrated into 1 mL by nitrogen. The concentrated solution was dropped on a high reflection glass window for LDIR detection after the ethanol volatilized.

2.1.4 MPs detected by LDIR

A LDIR imaging system (Agilent 8700, Agilent Technologies Inc., Santa Clara, CA) equipped with Agilent Clarity software and library of Microplastics Starter 1.0.1 was used to identify the MPs, with spectral wavelengths of 975-1800 cm^{-1}. The standard spectra were derived from the determination of the LDIR imaging system to standards.

During LDIR detection, only particles with matching degree exceeding 65% were identified as MPs, and the detection limit was 10 μm.

2.2 Distribution characteristics of the AMPs concentration

From September 2021 to August 2022, the concentration of AMPs in Tianjin ranged from 200−463.9 n/m^3, with an average concentration of 335.1(Fig 2.4A). To date, AMPs concentrations have been reported worldwide, especially in Europe and East Asia[5, 20, 21]. The reported AMPs concentration depends largely on the resolution of the detection method. For example, when using a Raman microscope with a resolution of 2 μm, a concentration of 2502 n/m^3 was observed measurements in London[22]. When a micro-Fourier Transform infrared spectrometer (μ-FTIR) with a detection limit of about 11 μm was used, AMPs concentrations in the range of 0.17−6.20 n/m^3 were measured in Guangzhou and Shanghai, China[5, 23]; Seoul, Korea[24]; Paris, France[25]; and Southern California, USA. Previous studies have shown that the concentration of AMPs generally increases rapidly with the decrease of their size[22]. In this study, the 10−20 μm AMPs detected in Tianjin accounted for approximately 50% of all MPs particles at a concentration of 102.8−298.6 n/m^3, which is of the same order of magnitude as the AMPs concentrations reported in London[22] in the same particle size range (Figure 2.4A).

The concentration of AMPs of Toyama ranged from 163.9-293.1 n/m^3, with an average of 217.8 n/m^3 (Fig 2.4B), significantly lower ($p<0.05$) than that of Tianjin, which has a higher population density. Mandalgobi showed the lowest population density among all the sampled sites, as well as the lowest AMPs concentration (109.8−183.9 n/m^3, with an average concentration of 150.0 n/m^3, Fig 2.4C) Human activities, such as the discharge of laundry wastewater and municipal sewage[26, 27] and the improper disposal of industrial waste and wastewater[28, 29], and the wear and tear of automobile tires[30], can all result in large amounts of MPs entering the environment. In addition, wind[31], turbulence generated during vehicle driving[32], and mechanical force generated by soil turning in farmland[33, 34] will provide the power for MPs in the environment to enter the atmosphere. Therefore, AMPs concentration is often higher in areas with higher population density[22, 35].

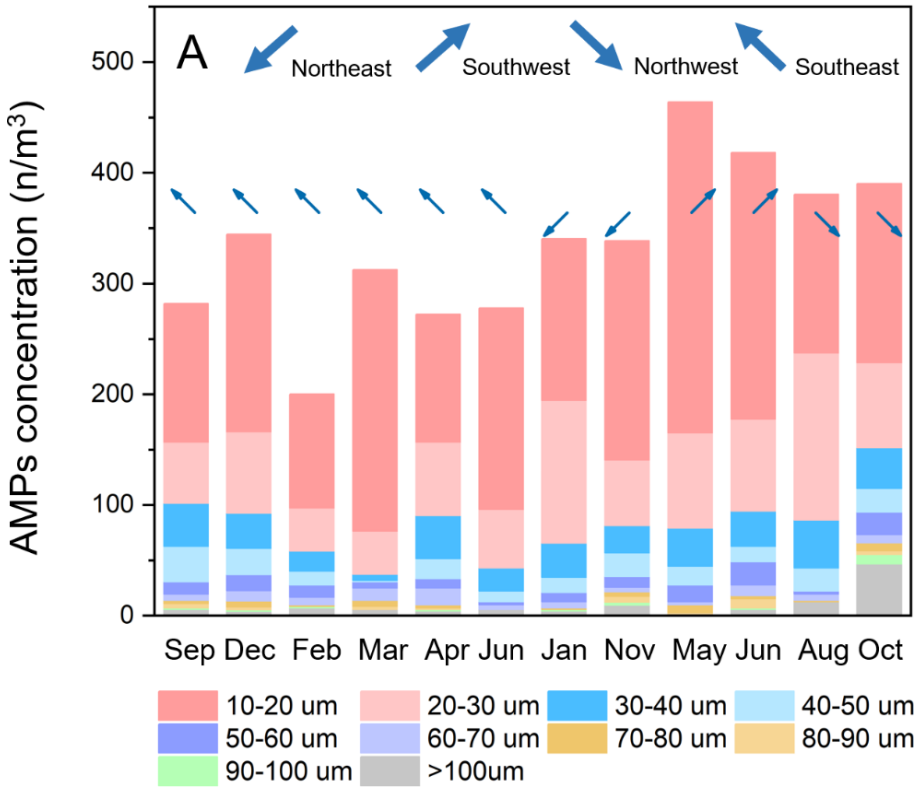
A
Northeast
Southwest
Northwest
Southeast
AMPs concentration (n/m3)
0
100
200
300
400
500
Sep Dec Feb Mar Apr Jun Jan Nov May Jun Aug Oct
10-20 um
20-30 um
30-40 um
40-50 um
50-60 um
60-70 um
70-80 um
80-90 um
90-100 um
>100um

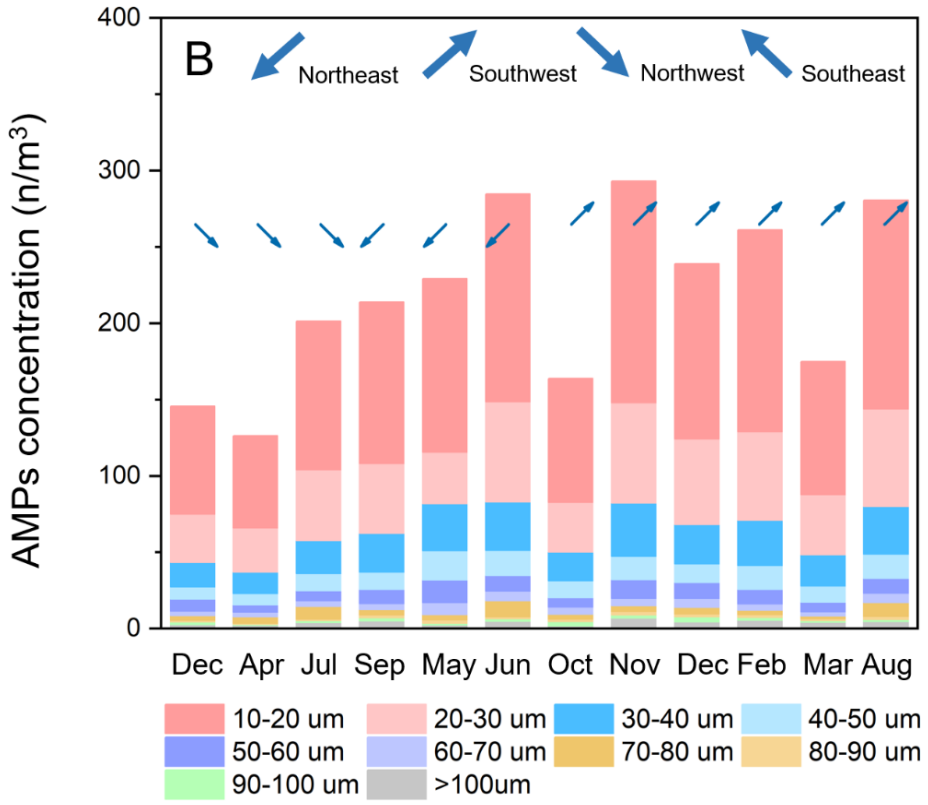
B
Northeast
Southwest
Northwest
Southeast
AMPs concentration (n/m3)
0
100
200
300
400
Dec Apr Jul Sep May Jun Oct Nov Dec Feb Mar Aug
10-20 um
20-30 um
30-40 um
40-50 um
50-60 um
60-70 um
70-80 um
80-90 um
90-100 um
>100um

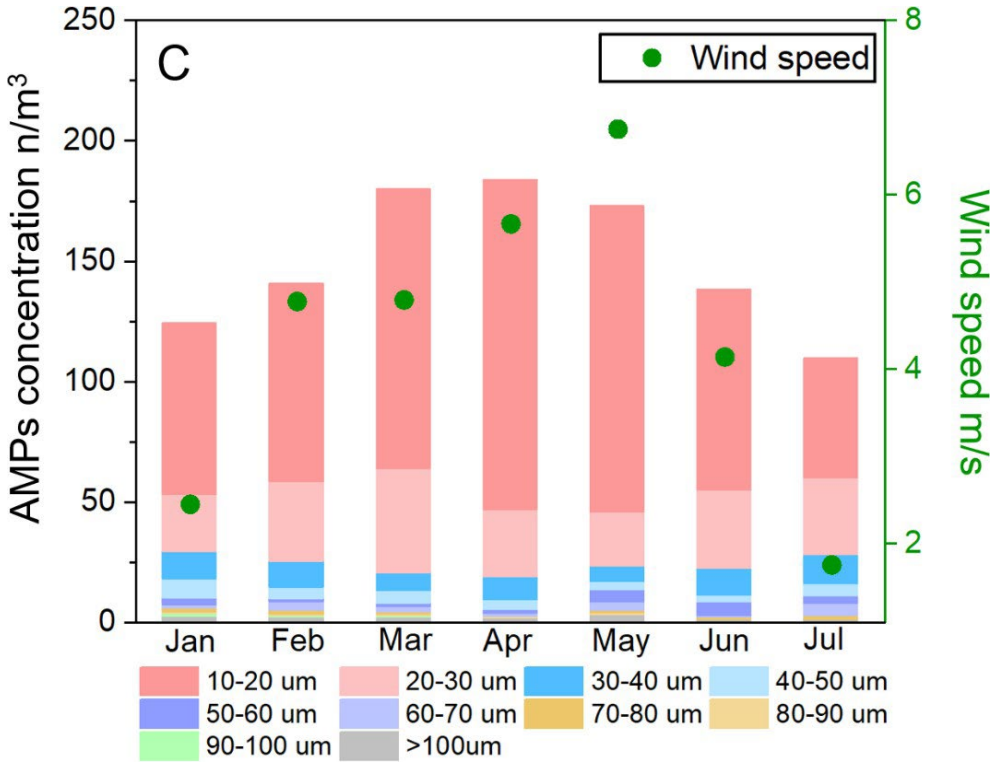

Figure 2.4 Monthly concentrations of AMPs of Mandalgobi (A), with green dots representing the average wind speed during sampling time. Monthly concentrations of AMPs of Tianjin (B) and Toyama (C), with blue arrows representing the wind direction during sampling time.

There are significant differences of AMPs concentration over ocean and land[23], thus , wind direction is likely to affect the concentration distribution of AMPs in coastal areas [36, 37]. In this study, principal component analysis (PCA) was used to investigate the influence of wind on AMPs concentration in East Asian cities. There was no significant correlation was found between wind speed and AMPs concentration of Tianjin and Toyama, although there was an acute angle between the vectors representing wind speed and AMPs concentration (Fig 2.5A and B). However, it was found that when the southeast wind prevailed, the AMPs concentration in Tianjin was significantly lower than that in other local periods ($p<0.05$, Fig 2.4A) and when the northwest wind prevailed, the AMPs concentration in Toyama was significantly lower than that in other periods ($p<0.05$, Fig 2.4B). The results of PCA analysis showed that the AMPs concentration in Tianjin was significantly negatively correlated with the frequency of southeast wind ($p<0.05$, Fig 2.5A), while the AMPs concentration of Toyama was significantly negatively correlated with the frequency of northwest wind ($p<0.05$, Fig 2.5B). The Bohai Sea located is the southeast of Tianjin, and the Sea of Japan is located in the northwest of Toyama. Thus, winds blow form the ocean will dilute the concentration of AMPs over the city.

The AMPs concentration in Mandalgobi did not show a significant correlation with wind direction, but was more consistent with the variation trend of wind speed except

May (Figure 2.4C). In addition, positive correlations ($p<0.05$) between AMPs concentrations and the frequency of wind speed >3m/s, >4m/s and >5m/s were observed (Fig 2.5C). In remote areas, the concentration of MPs in dust-fall is significantly positively correlated with wind speed, indicating that MPs from pollution sources can be transported over long distances by wind[7, 37, 38]. Therefore, the correlation between the AMPs concentration and wind speed of Mandalgobi indicates that there may be external input of AMPs.

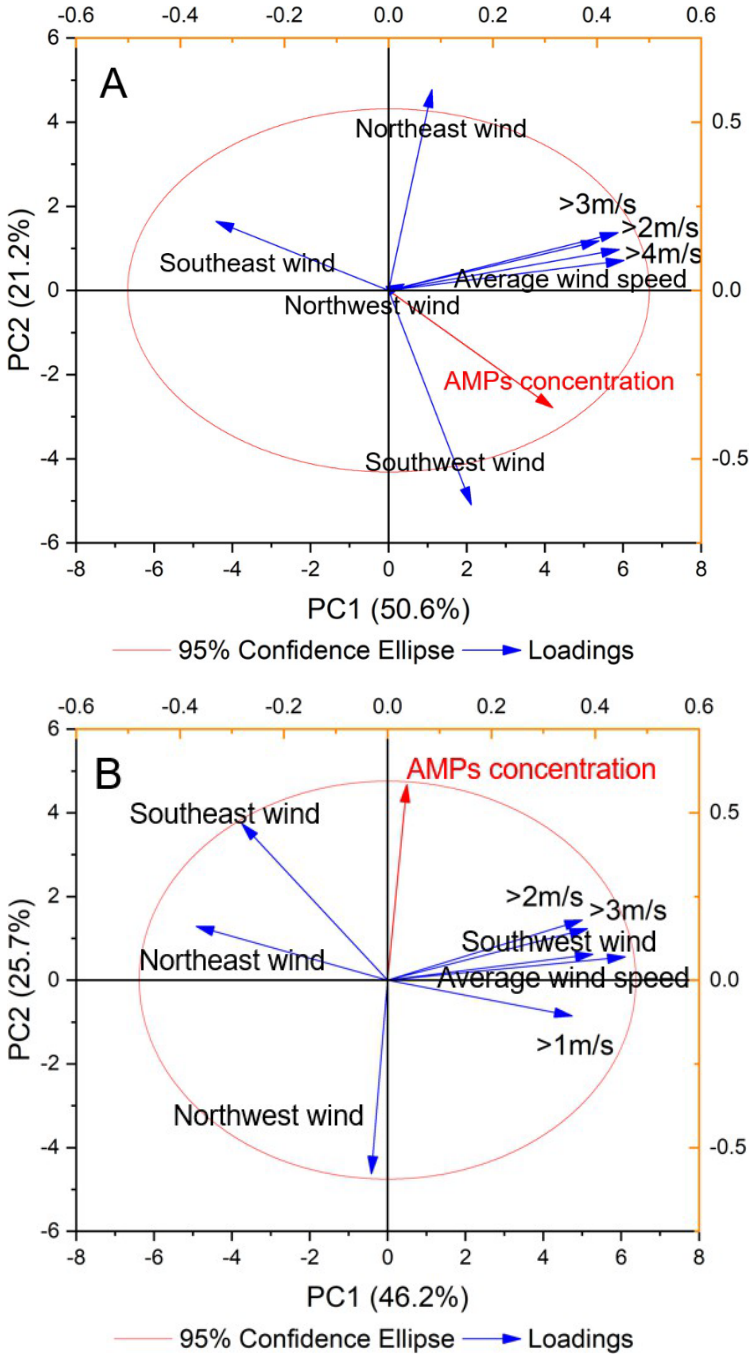

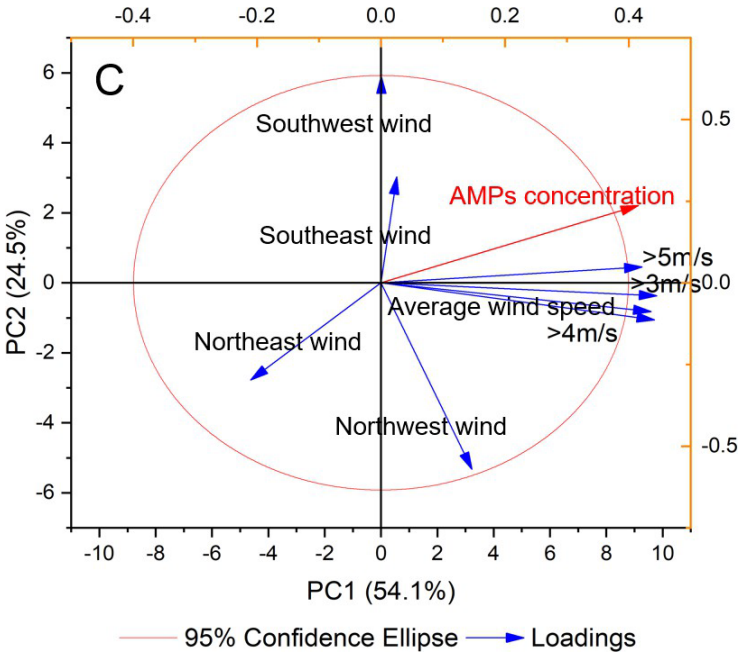

Figure 2.5 Principal component Analysis (PCA) based on the AMPs concentration, wind speed and wind direction of Mandalgobi (A), TIanjin (B) and Toyama (C). An acute angle between the vectors represents a positive correlation, while an obtuse angle represents a negative correlation.

The average AMPs concentration of Hohhot, Tianjin and Toyama on clean days was 346.5±15.5 n/m^3, 426.4±27.8 n/m^3 and 248.4±11.3 n/m^3, respectively (Fig 2.6). Compare to that, a lower AMPs concentration was found in Hohhot and Tianjin during the dust event (221.1 n/m^3 and 173.1 n/m^3, respectively, Fig 2.6), while the AMPs concentrations of Toyama were similar on both dust and clean days.

The wind speed of Hohhot and Tianjin during the dust period was 6.9 m/s and 6.3 m/s, respectively, which was significantly higher than that on clean days (3.0 m/s and 2.7 m/s, Fig 2.6). In contrast, the wind speed of Toyama during the dust event was similar to that on clean days (2.5 m/s and 2.2 m/s, Fig 2.6). Strong winds can disperse AMPs over cities, which may lead the decrease in AMPs concentrations.

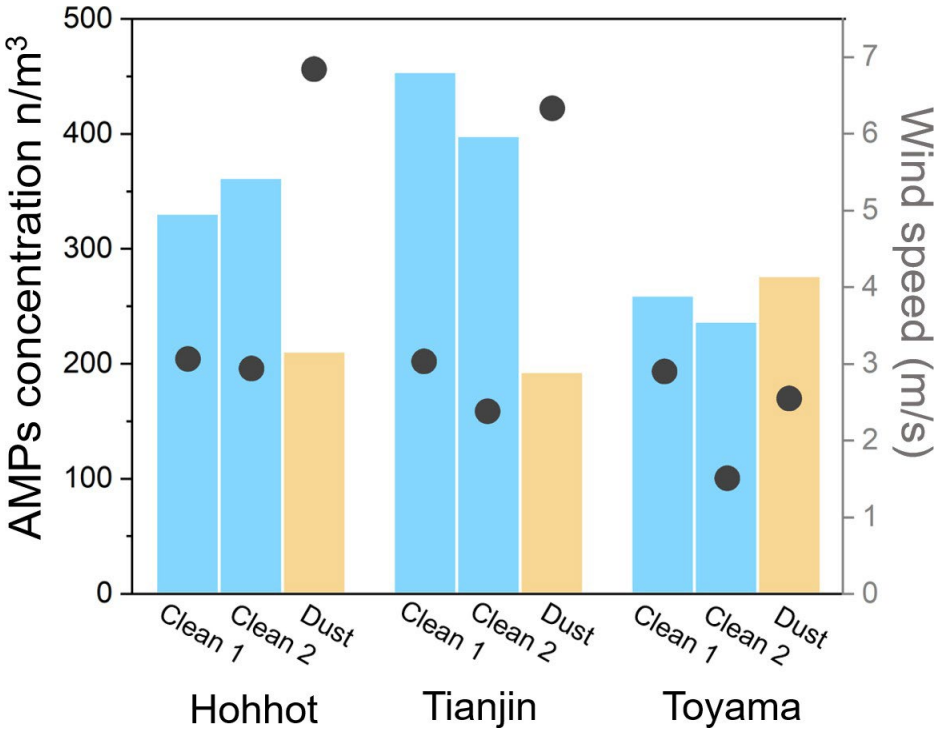

Figure 2.6 AMPs concentrations and average wind speeds (indicated by the dark gray dots) of Hohhot, Tianjin and Toyama on clean day and during dust events.

2.3 Distribution characteristics of the AMPs deposition flux

The average annual deposition flux of AMPs of the sampling cities was positively correlated with local population density ($p<0.05$). More human activities may lead to more MPs entering the environment. These MPs can be carried into the atmosphere by wind, turbulence generated by car travel, and mechanical forces from soil turnover in farmlands, ultimately resulting in an increased amount of MPs in the atmosphere that settle to the ground.

Quarterly deposition flux of AMPs in Mandalgobi, Hohhot, Tianjin and Toyama were 1848−7486 n/m^3, 4932−6089 n/m^3, 13575−25730 n/m^3 and 17726−265343 n/m3, with an average value of 4667 n/m^3, 5445 n/m^3, 21131 n/m^3 and 25052 n/m^3, respectively (Fig 2.7). The average annual deposition flux of AMPs of the sampling cities was positively correlated with local population density ($p<0.05$). More human activities may lead to more MPs entering the environment. These MPs can be entrained into the atmosphere by wind, turbulence generated by car and other mechanical forces[33, 34], resulting in an increased amount of MPs in the atmosphere and then settle on the ground[32].

The deposition flux of AMPs in Mandalgobi was positively correlated with the average wind speed ($p<0.05$, Fig 2.7 B). The deposition flux of AMPs in Tianjin was negatively correlated with the frequency of southeast wind ($p<0.05$, Fig 2.7 D), and the

deposition flux of AMPs in Toyama was negatively correlated with the frequency of northwest wind ($p<0.05$, Fig 2.7E). These results are consistent with the correlations between the AMPs concentration and meteorological factors in Mandalgobi, Tianjin and Toyama (Fig 2.5A to C). In addition, a negative correlation was observed between the AMPs deposition flux and rainfall (amount and events) of Hohhot ($p<0.05$, Fig 2.7 C). Although rainfall can promote the deposition of AMPs[5], once AMPs enter the aquatic environment, they are less likely to resuspend in the short term, which may ultimately lead to a decrease in the deposition flux of AMPs[39].

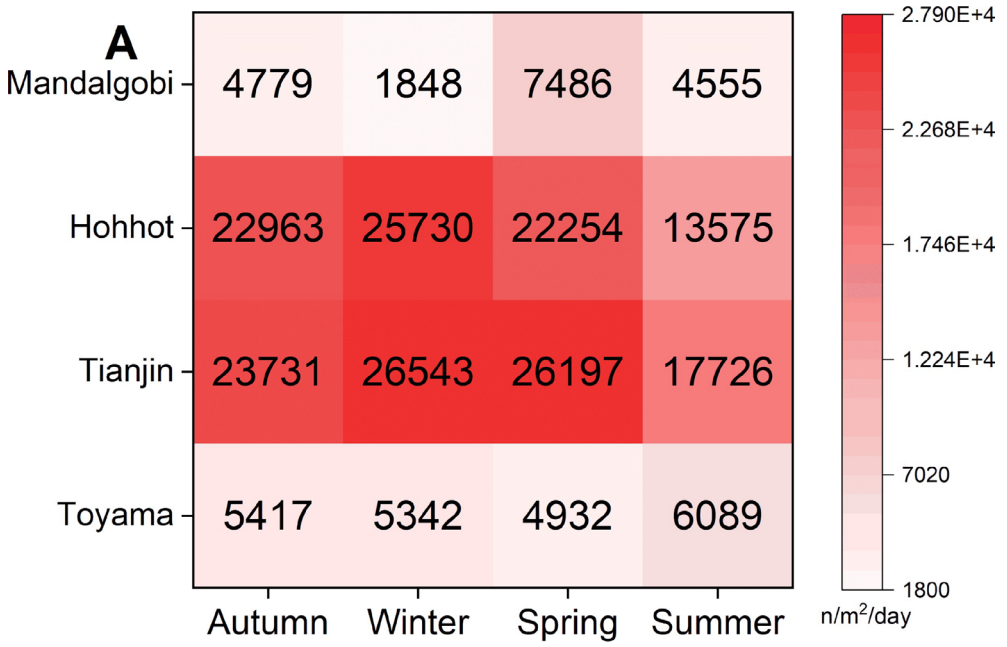

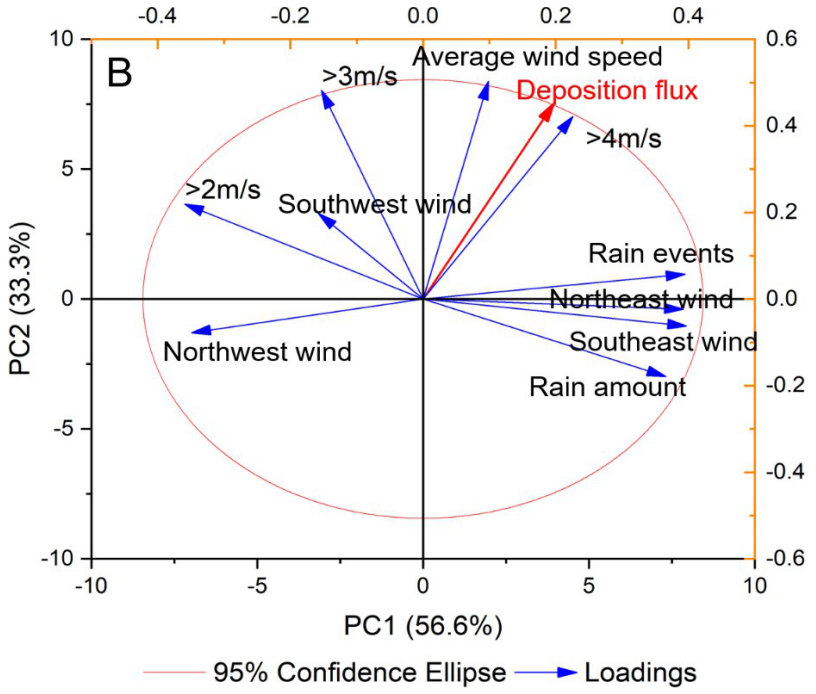

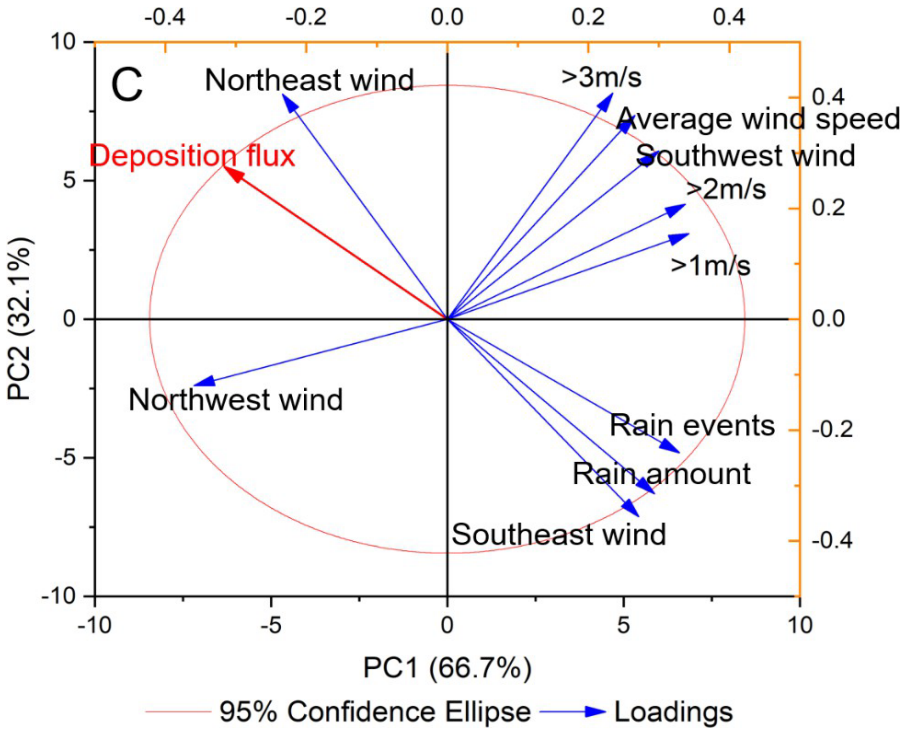
C
Northeast wind
>3m/s
Average wind speed
Southwest wind
Deposition flux
>2m/s
>1m/s
Northwest wind
Rain events
Rain amount
Southeast wind
PC2 (32.1%)
PC1 (66.7%)
95% Confidence Ellipse
Loadings

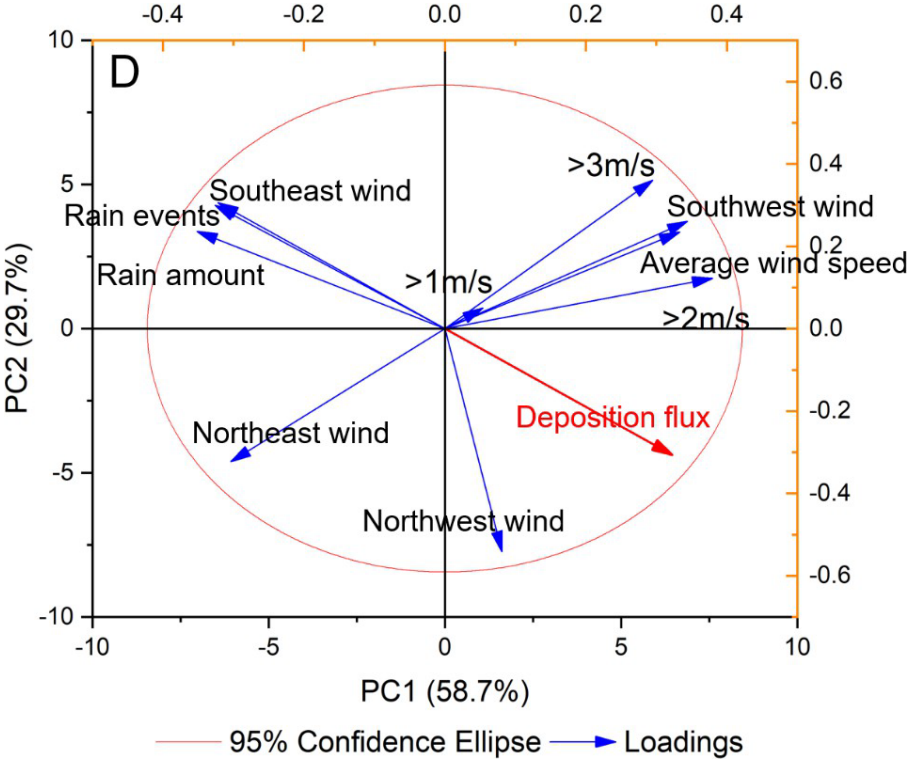
D
Southeast wind
Rain events
>3m/s
Southwest wind
Rain amount
>1m/s
Average wind speed
>2m/s
Deposition flux
Northeast wind
Northwest wind
PC2 (29.7%)
PC1 (58.7%)
95% Confidence Ellipse
Loadings

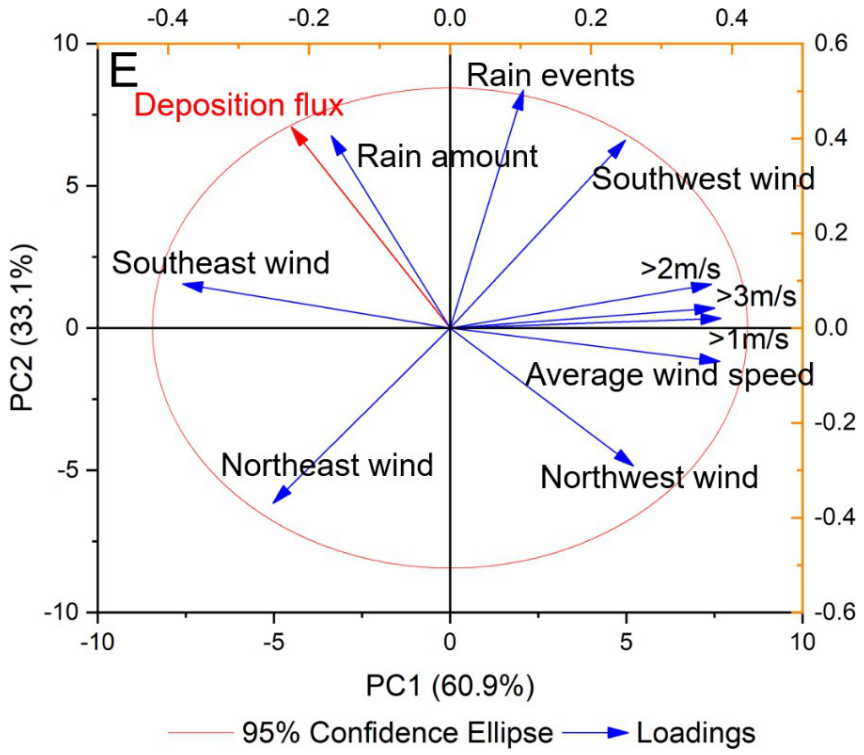

Figure 2.7 Quarterly deposition fluxes of AMPs of sampling cities (A). Principal component Analysis (PCA) of Mandalgobi B), Hohhot (C), Tianjin (D) and Toyama (E), based on the deposition flux of AMPs, wind speed, wind direction, rain fall events and rainfall amount. An acute angle between vectors representing a positive correlation, while an obtuse angle representing a negative correlation.

3 Assessing the external input of MPs based on polymer composition and aging characteristics

Composition of plastic polymers can be a tool to trace the commodity origin of MPs[8, 40]. For example, the polycarbonate (PC) MPs primarily come from hard plastic packaging shells, and the indoor polyethylene terephthalate (PET) MPs mainly origin from textiles[41]. Ratio of the mass concentration of PET and polyamide (PA) was applied to distinguish the textile and nontextile sources of MPs, and it is suggested that approximately 50% of indoor MPs may come from textile products[42].

Surface characteristic of environmental particles is also potential tool to trace the source of aerosol pollution. For example, the extent to which black carbon is coated by secondary aerosols, an indicator of the aging degree of black carbon, was used to verify the presence of long transported black carbon[14]. Similarly, the aging of MPs surface presents under the action of ultraviolet irradiation and microbial activity[40], and higher carbonyl index (CI), an indicator for assessing the degree of MPs aging[40, 43], may reflect the potential of long transport of MPs[43].

Theoretically the contribution of local and external MPs might be identified by the characteristics of MPs composition and aging degree, especially for areas where external pollution contributes significantly. In order to establish credible methods to assess the external input of MPs, Siziwang Banner twon (Sizi) and Hohhot city on the Mongolian Plateau, which located in the north and south of the Yinshan Mountains respectively, were selected as the research areas (Fig 3.1 A). The two areas are located in the East Asian monsoon region with a predominance of northwest wind. Sizi, a town with a population of about 200,000 and primarily engaged in animal husbandry, is surrounded by vast plains in all directions except the south, making it susceptible to the transport of atmospheric MPs from various directions except the south (Fig 3.1 B). Hohhot, the capital of the Inner Mongolia Autonomous Region, China, a heavily industrialized city with a population of approximately 3.5 million, is partially enveloped by the mountain range, which to some extent protects Hohhot from the external input of atmospheric MPs (Fig 3.1B).

In this study, outdoor dust was collected in Sizi and Hohhot, and the size distribution, composition and characteristics of surface functional groups of MPs were analyzed. Based on the composition and aging degree of MPs with different sizes, the external MPs was identified, and the methods for assessing the contribution of external input to region with low local MPs pollution was established.

3.1 Methods

3.1.1 Research area and sample collection

On September 6, 2021, a total of 20 outdoor dust samples were collected from Sizi (111.70 E, 41.53 N) and Hohhot (111.67 E, 40.76 N), respectively. The locations of sampling sites were shown in Fig 3.1B. Hohhot and Sizi are not typical regions with high river occurrence, and both areas fall under the temperate continental climate type with relatively low precipitation. For instance, in 2021, the annual precipitation in Hohhot and Sizi was 242.8 mm and 133.2 mm (https://data.cma.cn), respectively. Thus, the risk of MPs being input from surface runoff is low.

Hog bristle brushes were used to sweep the outdoor dust on the road (approximately 2 g for each). The collected dust samples were put into a paper bag lined with aluminum foil. After transported to lab, the samples were sieved through a 2 mm pre-washed metal sieve and then stored in a 4 ℃ refrigerator.

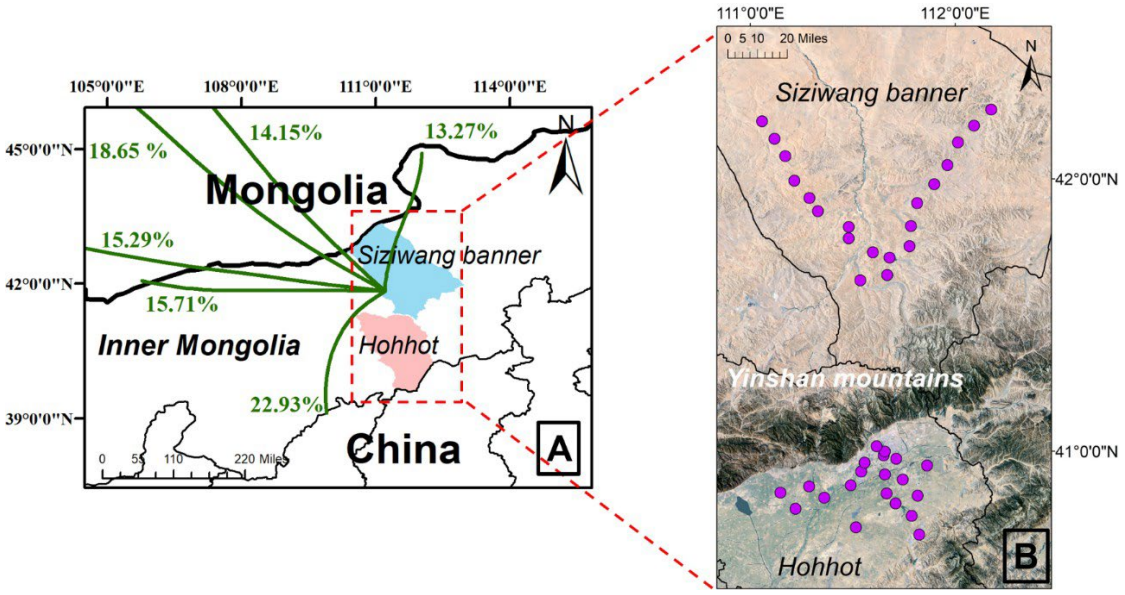

Figure 3.1 Map of sampling locations for outdoor dust. Two research areas, Siziwang Banner and Hohhot, are outlined in red dotted box (A) and magnified in the right image (B). The outdoor dust samples were collected in Siziwang Banner (n=20) and Hohhot (n=20), respectively, and the purple dots (B) represent the sampling location of each sample. The green curves shown in the left image represent the 24 h backward trajectories of air masses in Siziwang manner, with the percentage representing the proportion of the air mass in that direction to the total trajectories (A).

3.1.2 Sample pre-treatment and MPs detection

The MPs in the sieved outdoor dust samples (< 2 mm) was extracted by a digestion-flotation method. In brief, 0.2 g outdoor dust was accurately weighted, digested by H_2O_2 solution (30%), and the MPs in outdoor dust were floated by $ZnCl_2$ solution (52%). The separated particles were stored in 1mL of ethanol in a glass sample vial. The ethanol solution was dropped on a high reflection glass window for LDIR detection after the ethanol volatilized.

The detection of MPs is the same as in 2.1.3. LDIR can provide the infrared absorption spectrum of rach detected particle. As PE MP was detected in all of samples, CI of PE can be obtained[44] as the ratio of the absorbance area of carbonyl group (1680-1779 cm^{-1}) and the absorbance area of methylene (1420-1490 cm^{-1}) obtained by LDIR.

3.1.3 Air masses trajectory clustering

The Hybrid Single-Particle Lagrangian Integrated Trajectory (HYSPLIT) model, which has been widely used to trace the source of atmospheric MPs[45] , was used to illustrate the backward trajectories of air masses arrived at the south of Mongolia Plateau during September 2020 to August 2021. The model was run in backward mode for 24 h simulations, with 1-h time intervals. Calculated backward trajectories were

clustered into six main trajectories (Fig 3.1A) by MeteoinfoMap 2.2.4 (China)[46], representing the main source directions of the air masses.

3.2 Concentration and size distribution of MPs in the outdoor dust

In the outdoor dust of Hohhot, 61000−102250 n/g of MPs were detected, with an average of 78625 n/g (Fig 3.2A). In comparison, significantly lower (p<0.05) MPs concentrations, 30500−60250 n/g with an average of 42888 n/g, were detected in Sizi (Fig 3.2A). MPs in outdoor dust is commonly positively correlated with local population[47], which can explain the difference of MPs concentration in Hohhot and Sizi.

Totally, the MPs concentrations increased with the decrease of MPs size (Fig 3.2B). However, it is worth noting that the proportion of MPs below 25 μm of Size (64-71%) was significantly higher (p<0.05) than that of Hohhot (49-62%) (Fig 3.2B). MPs below 25 μm are considered to have the potential for long-distance transport through atmosphere[8, 48], as more than 70% of observed MPs in western U.S. protected lands are smaller than 25 μm. Therefore, it suggests the MPs in Sizi are more prone to be affected by atmospheric input.

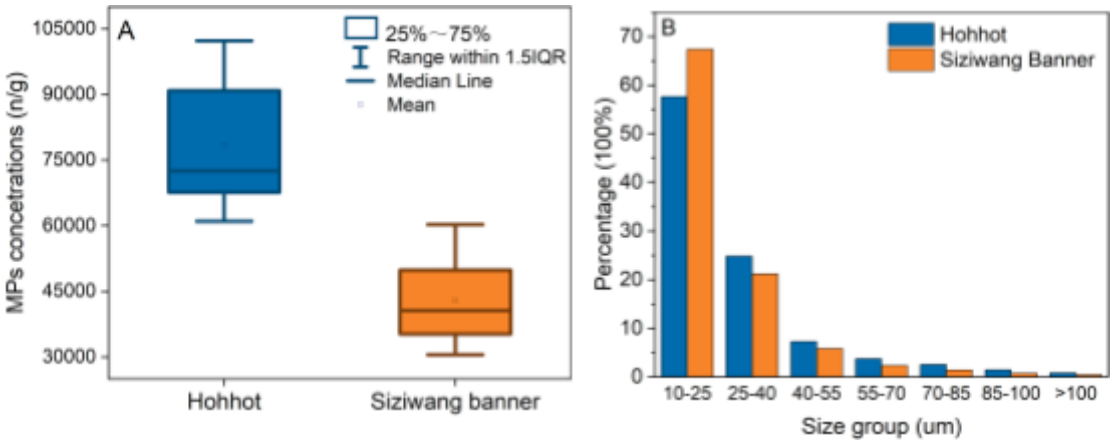

Figure 3.2. Concentration (A) and size distribution (B) of MPs in the outdoor dust of Hohhot and Siziwang banner.

3.3 Source of small sized MPs of Siziwang banner

To trace the atmospheric input of MPs in Sizi, the HYSPLIT model, a wildly used tool to explore the transport pathways of atmospheric particles[7, 37, 49], was employed to calculate air mass backward trajectories in Sizi. It is indicated that the air mass mainly came from the northwest direction, accounting for 50% of the total air mass sources (Fig 3.3A). Moreover, compared to the air mass from other directions, the air mass from the northwest showed the longest transport distance, reaching up to approximately 1000

km within 24 hours. This indicates that atmospheric MPs from the northwest may undergo long-distance transport.

The flat Mongolian Plateau is located to the northwest of Sizi. Due to the obstruction of the Yinshan Mountains (Fig 3.3), the small atmospheric MPs from the northwest tend to settle on the plain of Sizi after long-distance transport, rather than further transport to Hohhot.

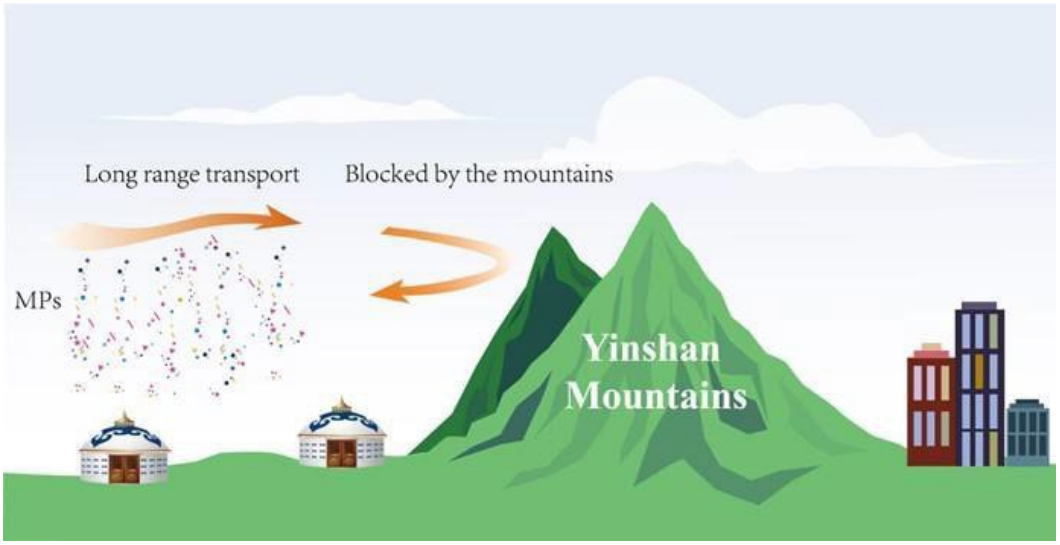

Figure 3.3 Representation of air masses carrying MPs for long-distance transport that are blocked by the Yinshan Mountains.

3.4 A composition based method to distinguish the external MPs.

A total of 26 types of polymers were identified and 25 of them were presented in both Sizi and Hohhot (Fig 3.4). Similar polymer composition distribution was observed in small and large MPs in outdoor dust of Hohhot, and the top three polymers were PET, PA and PC, accounting for 37.8%, 43.1% and 42.9%, respectively (Fig 3.4A). Consistent distribution characteristics of polymer components were also observed in the large MPs of Sizi (Fig 3.4A). However, it seems that the composition distribution of the small MPs of Sizi varied greatly. For example, polypropylene (PP) is the third most abundant polymer in the small MPs of Sizi (Fig 3.4A), accounting for ~10% of total detected MPs. Smaller MPs are more easily transported in the environment. Therefore, in the areas more heavily polluted by external sources, the small sized MPs should be more affected than the large sized MPs.

The differences in the distribution of polymer composition can be further identified by a principal coordinate analysis (PCoA). The fractions of 26 plastic polymers in each outdoor dust sample are considered as 26 properties of this sample, which was

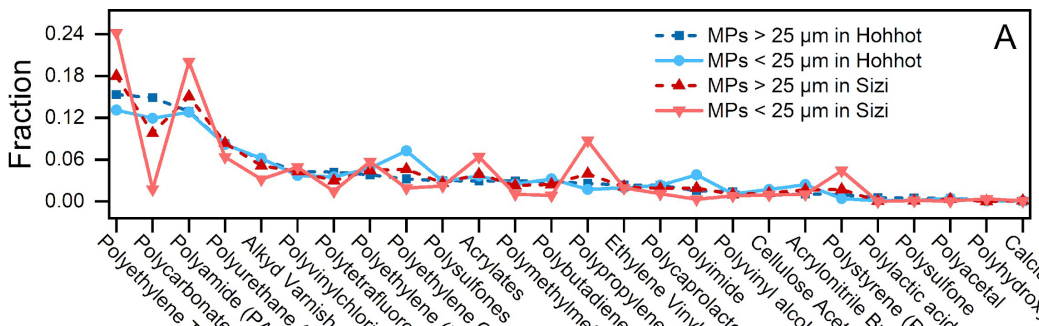

described as the "composition community" in Fig 3.4B and C. Based on the 20 outdoor dust samples of each group (large MPs of Hohhot, small MPs of Hohhot, large MPs of Sizi, small MPs of Sizi), 20 composition communities of MPs were obtained, respectively. According to the β diversity of composition communities shown by PCoA (Fig 3.4B and C), no significant difference of MPs composition presented between the large and small MPs of Hohhot (p>0.05, Fig 3.4B), while the composition structure of small MPs of Sizi was significantly different compared to the large MPs (p<0.05, Fig 3.4C). This suggests the heterologous pollution of small and large MPs in Sizi.

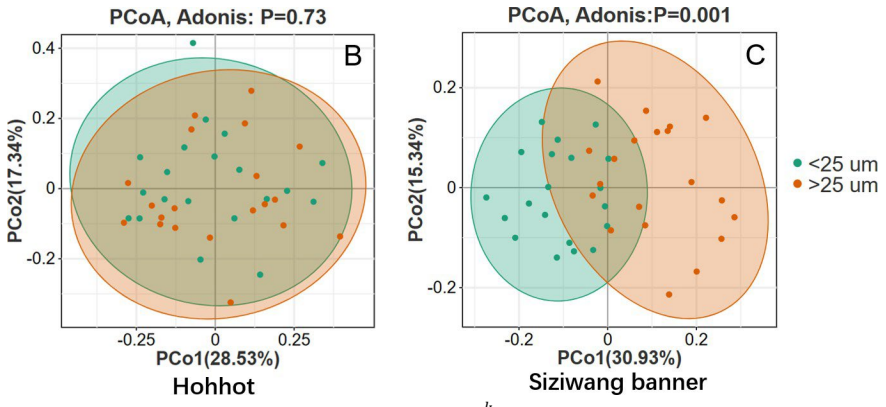

Figure 3.4 The polymer composition distribution of large sized (>25 μm) and small sized (<25 μm) `MPs in Hohhot and Sizi banner (A). β diversit of "composition communities" of MPs between large and small MPs in Hohhot (B) and Sizi banner (C), with each green dot (or each orange dot) represents a composition of 26 polymers in one sample.

Bray-Curtis similarity index (BCs), a tool to evaluate the species similarity between two ecosystem based on the relative abundance of species, was cited to quantify the difference of composition between the large and small MPs in Hohhot and Sizi. A composition fraction−based BCs (Comp−BCs) between large MPs and small MPs groups can be calculated as follows,

$$Comp\text{-}BCs = 1 - \frac{\sum_{t=1}^{k} \left| f_{t(L)} - f_{t(S)} \right|}{\sum_{t=1}^{k} \left(f_{t(L)} + f_{t(S)} \right)} \quad \text{(eq.1)}$$

where $f_{t(L)}$ and $f_{t(S)}$ are the values of fractions (f) of each polymer composition t in large (L) and small (S) MPs groups, respectively; and k is the number of types of polymers, that is 26 in this study. The Comp-BCs ranges from 0 to 1, with closer to 1 indicating that the objects being compared are more similar. Comp−BCs of large and small MPs in Hohhot and Sizi were 0.90 and 0.76, respectively, validating that large and small MPs of Sizi may be heterologous.

3.5 A CI based method to distinguish the external MPs

Changes of functional groups on the surface of MPs due to environmental aging can also be used to characterize environmental MPs. Based on the spectrum of LDIR of PE MPs, a significant higher average CI of PE in Sizi (1.00±0.56) than that in Hohhot (0.82±0.56) (p<0.01) was found. For the large sized PE (>25 μm) in Sizi and Hohhot, their average CI were equal to 0.82 (Fig 3.5), which is similar to the average CI of small sized PE (<25 μm) in Hohhot (0.83). Similar median CI values were also obtained for MPs of these three groups, which were 0.63 and 0.67 for the large sized PE in Sizi and Hohhot, and 0.66 for the small sized PE in Hohhot (Fig 3.6). In comparison, significantly higher CI of small sized PE in Sizi (average: 1.08; median: 1.13) was observed (Fig 3.5, Fig 3.6), exhibiting a different distribution pattern compared with the other three MPs groups (Fig 3.6). The different CI of small sized PE in Sizi should be attributed to the plastic aging during their long-distance transport[43]. MPs below 25 μm are potential for long-distance transport thus can be transported in the air to Sizi and blocked by the Yinshan Mountains (Fig 3.3). As a result, these small atmospheric MPs settle in Sizi rather than affecting Hohhot.

Bray-Curtis similarity index of CI (CI-BCs) between the large and small PE MPs can be calculated as eq.3,

$$CI - BCs = 1 - \frac{\sum_{i=1}^{k} \left| f_{i(L)} - f_{i(S)} \right|}{\sum_{i=1}^{k} \left(f_{i(L)} + f_{i(S)} \right)} \quad \text{(eq.2)}$$

Where $f_{i(L)}$ and $f_{i(S)}$ are fractions (f) of each 0.1 interval range (i) of CI of PE in the large sized (L) PE group and the small sized (S) PE group, respectively; and k is the total interval number, that is 26 in this study because the CI of all target PE ranged between 0-2.6. $CI - BCs$ between large and small PE in Hohhot was 0.89, reflecting that the environmental aging experienced by small and large PE MPs in Hohhot is basically the same. Differently, $CI - BCs$ between the large and small PE in Sizi was 0.64, illustrating a more significant difference in the aging degree between the large and small sized PE. The difference of CI between large and small PE can served as an indicator of the external contribution to total MPs, as the atmospheric transport efficiencies of different types of MPs are almost the same[10]. Together with the relatively small Comp-BCs of MPs in Sizi (0.77), important contribution of the external small MPs input to Sizi can be validated.

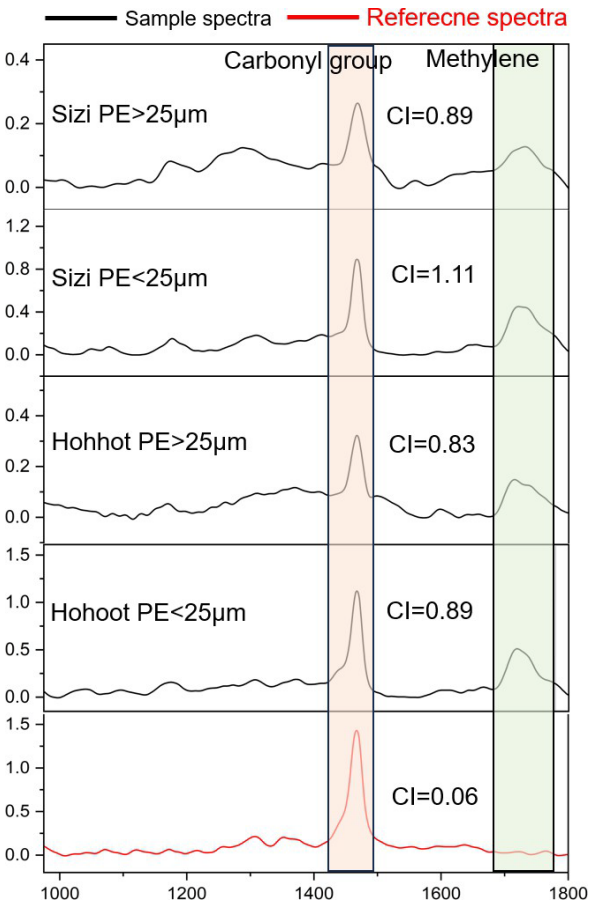

Figure 3.5 LDIR spectra of reference PE and aged PE. The red line represents the spectrum of the standard PE, and the blackline represents the PE in outdoor dust collected in Siziwang banner and Hohhot.

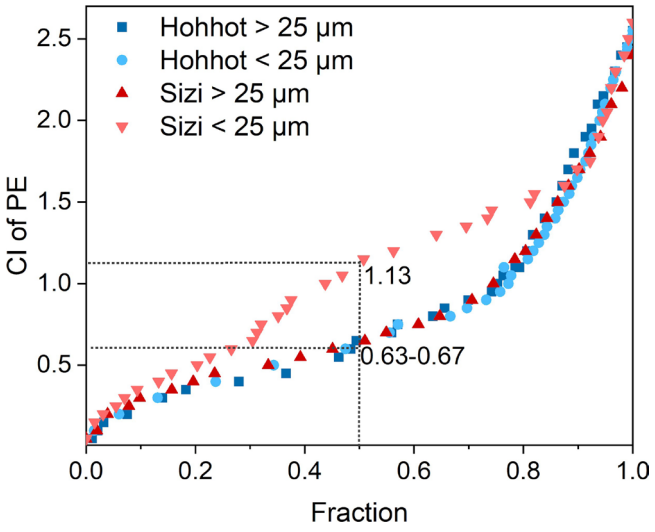

Figure 3.6 CI of PE with different sizes in Siziwang banner and Hohhot. The median CI of small sized PE (< 25 μm) of Sizi and Hohhot was 1.13 and 0.66, respectively, and the median CI of large sized PE (> 25 μm) was 0.63 and 0.67, respectively.

4 Evaluating the risk of long-distance transport of AMPs in East Aisa

4.1 The risk of long-distance transport of AMPs under conventional weather conditions

The Comp-BCs of MPs in the dust-fall of Mandalgobi, Hohhot, Tianjin and Toyama were 0.67−0.77, 0.67−0.85, 0.82−0.85 and 0.82−0.89, respectively (Fig 4.1A). Meanwhile, it was found that 69.4% to 75.8% of MPs were smaller than 25 μm (Fig 4.1A) in Mandalgobi, which was significantly higher ($p<0.05$) than that in other sampling sites (51.2−68.7%) (Figure 4.1A). The low Comp-BCs combied the high portion of small sized MPs indicate that Mandalgobi is vulnerable to external AMPs pollution. In addition, a higher CI of small sized PE was also observed in Mandalgobi ($p<0.05$, Fig 4.1B), which further validates the presence of external small sized MPs.

It is worth noting that, compared to other seasons, a significant lower Comp-BCs ($p<0.05$) and a significant higher CI of PE ($p<0.05$) were both found in the spring dust-fall of Hohhot (Fig 4.1B), indicating that local area is more likely to be polluted by external MPs during spring. Backward trajectories indicate that, compared to other seasons, a higher portion of air mass in spring (50%) of Hohhot were originated from the interior of the Mongolian Plateau (Fig 4.2 A to D). At the same time, it was found that the composition of small sized MPs in spring dust-fall of Mandalgobi and Hohhot was more similar than that in dust-fall of other seasons (Fig 4.3). All these results suggest a high risk of long-distance transport of AMPs from the interior of the Mongolian Plateau to the North China during the spring season.

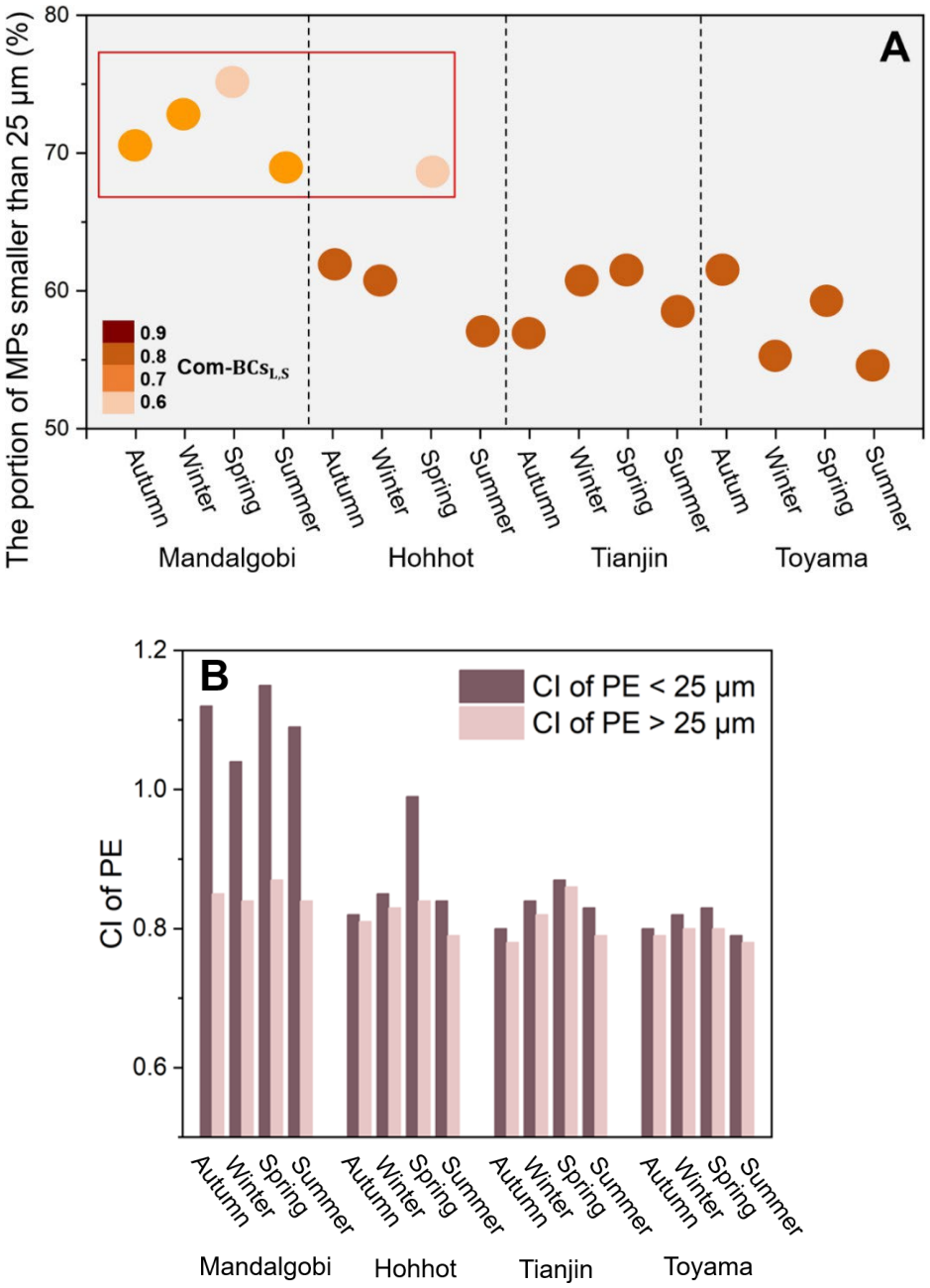

Figure 4.1 The Comp-based BCs index of MPs, which representing the composition differences between large sized MPs (> 25 μm) and small sized MPs (< 25 μm), in dust-fall samples (A). The CI of PE MP in dust-fall samples (B).

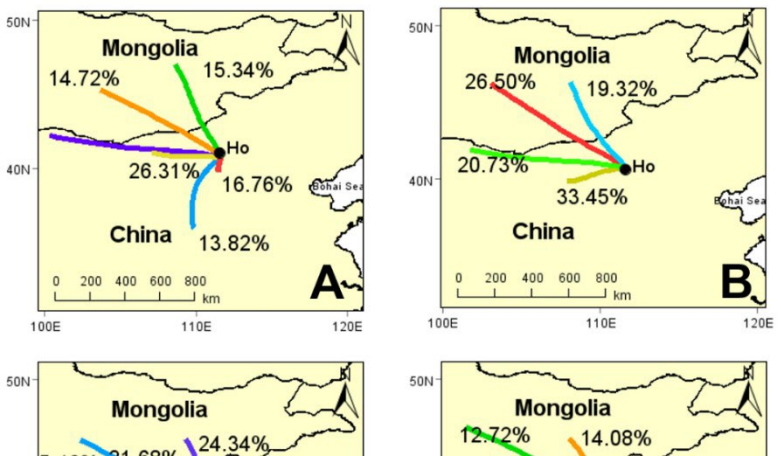

Figure 4.2 Backwards trajectories and their portions of Hohhot (HO) in Autumn (A), Winter (B), Spring (C) and Summer (D).

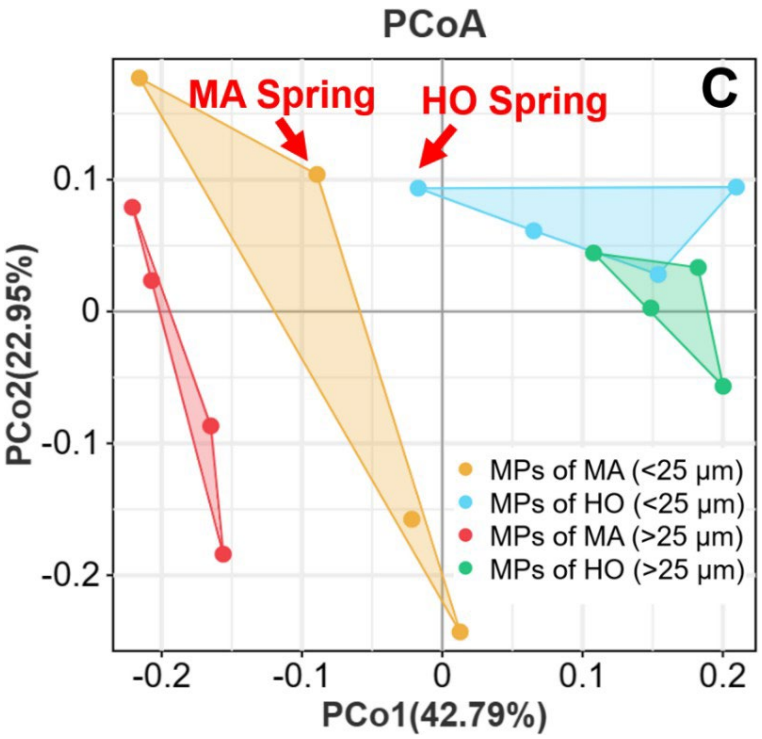

Figure 4.3 The principal coordinates analysis (PCoA) of the AMPs composition of Mandalgobi (MA) and Hohhot (HO). Each point in the PCoA plot represents a composition of small sized MPs or large sized MPs of a dust-fall sample. The closer the distance between two sample points, the more similar the composition of the microplastics they represent.

4.2 The risk of long-distance transport of AMPs during dust events

Based on the detection and analysis of suspended particulate samples, a low Comp-BCs was observed in Hohhot, Tianjin and Toyama during dust events (Fig 4.4A). Combined with the high CI of PE observed in these three cities during dust events (Fig 4.4B), the pollution of external MPs during dust event was validated.

Backward trajectories suggest that air masses in Hohhot and Tian during dust period were originated from the interior of Mongolian Plateau (Fig 4.5). Since there is no obvious source of MPs pollution between Hohhot and the China-Mongolia border, the external MPs of Hohhot during the dust period were likely originated from the interior Mongolian Plateau. The air mass of Toyama during the dust period passed through the East Asian continent and the Sea of Japan. Thus, it is likely that the external MPs of Toyama originated from the East Aisa continent.

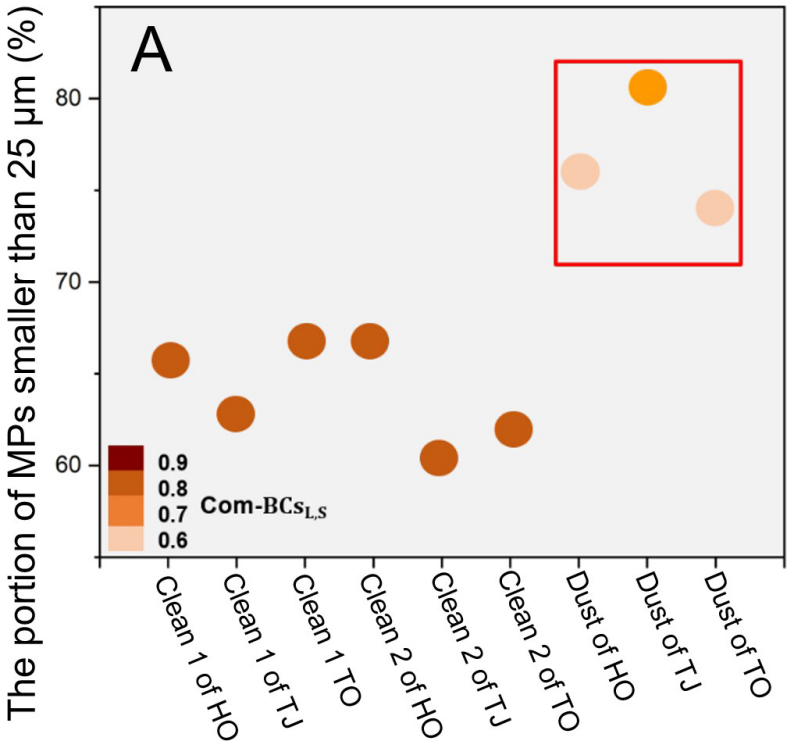
A
The portion of MPs smaller than 25 μm (%)
80
70
60
0.9
0.8
0.7
0.6
Com-BCs$_{L,S}$
Clean 1 of HO
Clean 1 of TJ
Clean 1 TO
Clean 2 of HO
Clean 2 of TJ
Clean 2 of TO
Dust of HO
Dust of TJ
Dust of TO

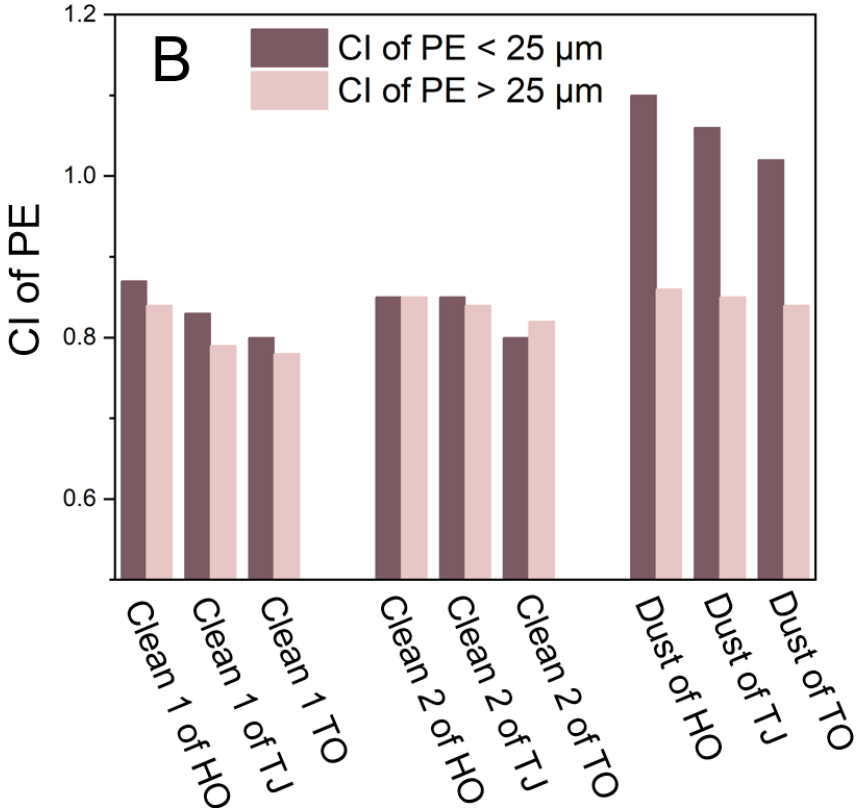
B
CI of PE < 25 μm
CI of PE > 25 μm
CI of PE
1.2
1.0
0.8
0.6
Clean 1 of HO
Clean 1 of TJ
Clean 1 TO
Clean 2 of HO
Clean 2 of TJ
Clean 2 of TO
Dust of HO
Dust of TJ
Dust of TO

Figure 4.4 The Comp-based BCs of AMPs on clean days and during dust events (A). The CI of PE of suspended particulate samples on clean days and during dust events (B). TO, TJ and HO represent Toyama, Tianjin and Hohhot, respectively.

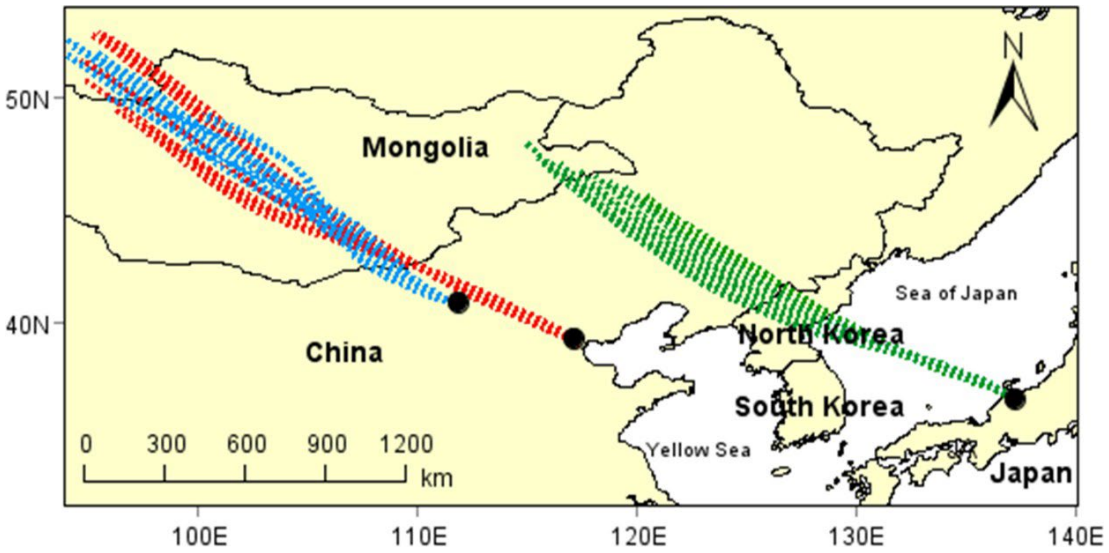

Figure 4.5 Backward trajectories of air masses for 24 hours at 1-hour intervals for Hohhot, Tianjin, and Toyama, during the sampling time of dust events.

5. Radiative forcing of AMPs in East Asia

5.1 Methods

For a given atmospheric height, aerosol direct radiative forcing (DRF) can be calculated based on the difference in net fluxes with and without aerosols. In this study, DRFs of AMPs at top of the atmosphere (TOA) and at the Earth's surface (ES) were calculated by Santa Barbara Discrete Ordinate Radiative Transfer (SBDART) model[50], a widely used model in estimating the radiative forcing of various aerosols[51-55]. Optical parameters of MPs used in SBDART include the spectral single scattering albedo (SSA), asymmetric factor (ASY) and aerosol optical depth (AOD). Aerosol optical properties are affected by the aerosol particle size distribution[56]. As the average size of MPs in Tianjin (35 μm, Fig 2.4A) is similar to that observed in a previous research (36 μm)[19], SSA and ASY, which are not affected by AMPs concentration and environmental variables, were cited directly from the previous study[19]. The AOD of AMPs can be obtained by following the steps below.

The vertical distribution of MPs below 10 km can be described as eq.1[19],

$$[MP]_{z} = N_{o} \times 0.3^{\frac{z}{10}} \quad \text{(eq.1)}$$

where z is height in kilometers above the ground, N_0 is the AMPs (n/m^3) concentration on ES, and $[MP]_z$ is MPs concentration (n/m^3) in the atmosphere at altitude z. Since the SBDART requires the inputs of optical parameters for boundary layer aerosols in order

to obtain the aerosol radiative forcing at TOA and ES, the variable z was set to 2 km in this study, representing the typical height of the boundary layer. A previous study showed that AMPs between 0 to 10 μm accounted for approximately 25% of the total AMPs[19]. Thus, the ES concentration of AMPs in this study was obtained by adding 25% to the concentration detected by LDIR. Then, the average atmospheric column concentration of MPs (N_{MPs}, n/m^3) can be calculated as eq.2,

$$N_{MPs} = \frac{\int_0^z [MP]_z dz}{z} \quad \text{(eq.2)}$$

After N_{MPs} was determined, the corresponding spectral absorbing coefficients (ABS) and scattering coefficients (SCA) can be obtained by multiplying the ABS and SCA in the source data (https://www.nature.com/articles/s41586-021-03864-x#MOESM10/) by N_{MPs} /N_{MPs} in the source data, as ABS and SCA change linearly with N_{MPs}. Then, the aerosol optical depth (AOD) of MPs, which is an important parameter to characterize the extinction properties of aerosols, can be calculated based on eq.3,

$$\mathrm{AOD}(\lambda) = \int_0^Z (ABS(\lambda) + SCA(\lambda))dz \quad \text{(eq.3)}$$

where λ is the wavelength.

In addition to the optical parameters, back ground parameters, including columnar ozone, surface albedo and columnar water vapor were also used in the SBDART model. By inputting the back ground parameters (Table 5.1 to 5.3) and spectral SSA, ASY and AOD, the integrated DFR of AMPs in shortwave range (0.25 to 4 μm) and longwave range (4 to 40 μm) can be obtained by SBDART model.

Table 5.1 The monthly varied columnar ozone, surface albedo and water vapor amount of Tianjin [a], during September 2021 to August 2022.

Month	Sep	Oct	Nov	Dec	Jan	Feb
columnar ozone (DU)	293.6	287.2	326.2	331.3	359.1	383.5
surface albedo	0.140	0.134	0.213	0.151	0.182	0.198
water vapor (cm)	2.532	0.979	0.617	0.363	0.362	0.253
Month	Mar	Apr	May	Jun	Jul	Aug

columnar ozone (DU)	350.9	347.0	354.1	332.1	307.8	292.8
surface albedo	0.168	0.151	0.151	0.151	0.155	0.151
water vapor (cm)	0.498	0.553	0.357	0.797	3.818	3.303

[a]Columnar ozone was obtained from Ozone Monitoring Instrument, surface albedo was obtained from ERA5-LAND and columnar water vapor was obtained from AERONET (Xianghe and Beijing stations). For water vapor, the data in principle came from the observation station closest to the sampling location. When data from the nearest station was missing, the data from another neighboring observatory was used as a supplement.

Table 5.2 The monthly varied columnar ozone, surface albedo and water vapor amount of Toyama, during January 2022 to June 2022.

Month	Jan	Feb	Mar	Apr	May	Jun
columnar ozone (DU)	337.8	360.3	348.6	333.6	333.4	326.0
surface albedo	0.482	0.478	0.355	0.186	0.124	0.124
water vapor (cm)	0.605	0.571	0.768	0.936	1.455	2.914

Table 5.3 The monthly varied columnar ozone, surface albedo and water vapor amount of Mandalgobi, during January 2022 to June 2022.

Month	Jan	Feb	Mar	Apr	May	Jun
columnar ozone (DU)	373.7	402.2	373.9	356.2	348.4	329.3
surface albedo	0.264	0.274	0.257	0.291	0.244	0.237
water vapor (cm)	0.186	0.150	0.260	0.373	0.513	1.047

5.2 DRF of AMPs in Tian throughout a year

Based on the AMPs observed in Tianjin from September 2021 to August 2022 (Fig 2.4A), the shortwave DRFs (DRF_{SW}) of AMPs were calculated by SBDART model as -0.03 to -0.21 W/m^2 at TOA and -0.07 to -0.44 W/m^2 at ES in Tianjin, China (Fig 5.1A and B). Meanwhile, the longwave DRFs (DRF_{LW}) of AMPs were calculated as 0.03 to 0.18 and 0.16 to 0.99 W/m^2 at TOA and ES, respectively (Fig 5.1A and B). Negative DRF_{SW} and positive DRF_{LW} suggest that AMPs led to a cooling effect in the shortwave band and a warming effect in the longwave band. This can be explained by the optical properties of polymers, i.e. MPs scattering radiation of shortwave and absorbing radiation of longwave[19].

The annual net AMPs DRF with different directions at ES and TOA, i.e. 0.402 $\pm$0. 256 W/m^2 at ES and -0.002$\pm$0. 016 W/m^2 at TOA were obtained (5.1 A and B). The net DRF at ES was positive in most months (0.10 to 0.72 W/m^2) except for that in July and August (-0.04 and -0.09 W/m^2, respectively) (Fig 5.1B). In contrast, the net DRF at TOA demonstrated greater uncertainty in the direction of DRFs, with half of the months being negative (-0.01 to -0.03 W/m^2) and half being positive (0.01 to 0.03 W/m^2) (Fig 5.1 A). AMPs can scatter shortwave radiation (RAD_{SW}) of solar radiation[19], thus cause a negative DRF_{SW} at ES. The absorption of longwave radiation (RAD_{LW}) of ground by AMPs can cause positive radiative forcing at ES[19]. The DRF_{LW} is larger than DRF_{SW} at ES, thus causing a positive net DRF. With the increased altitude, the DRF_{LW}

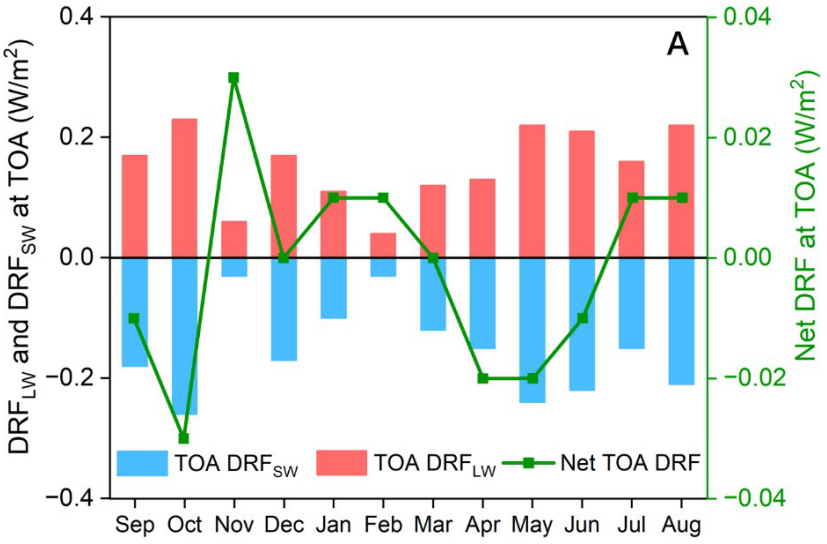

changes more rapidly since longwave radiation (RAD_{LW}) is sensitive to water vapor and decreased temperature[57]. As a whole, DRF_{SW} and DRF_{LW} of similar magnitude were obtained at TOA, resulting in a small net DRF with uncertain signs (Fig 5.1A).

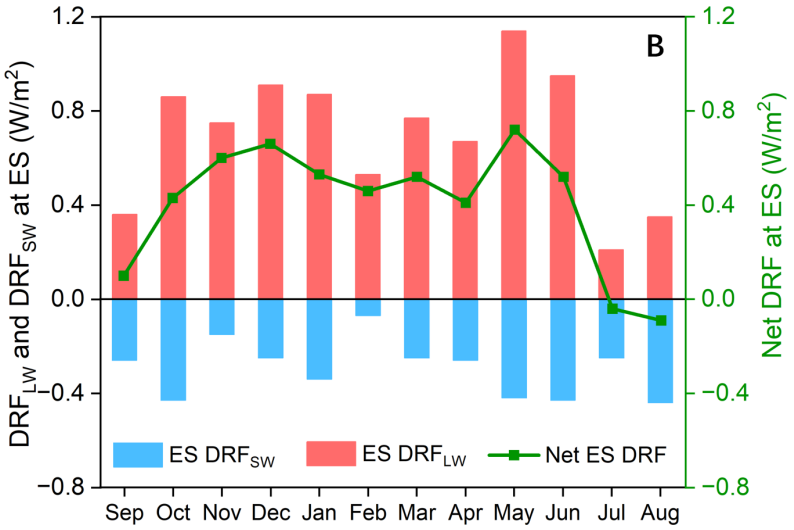

Figure 5.1 Monthly variation of shortwave DRF (DRF_{SW}), longwave DRF (DRF_{LW}), and net DRF at TOA (A) and ES (B).

Columnar ozone, water vapor, and surface albedo can affect the radiative fluxes, thus are important in estimating aerosol DRF[54]. Influence of these parameters on the absolute value of AMPs DRF was analyzed (Fig 5.2). All DRFs were significantly positively correlated with AMPs concentration (Spearman's correlation, $p< 0.05$, Fig 5.2). Therefore, the lowest DFR_{SW} at TOA and ES (-0.03 and -0.07 W/m^2, respectively, Fig 5.1A and B) and the lowest DFR_{LW} at TOA (0.04 W/m^2, Fig 5.1A) were all observed in February in Tianjin, which showed the lowest detected AMPs concentration (Fig 2.4A).

A negative correlation was observed between DRF_{LW} at ES and water vapor amount (Fig 5.2). Although DRF_{LW} at ES was not significantly correlated with water vapor amount (Spearman's correlation, $P>0.05$), it is worth noting that months with highest water vapor (2.532 to 3.818 cm in July to September, Table 5.1) showed the lowest ES DRF_{LW} (0.21 to 0.36 W/m^2, Fig 5.1B) in the whole year, while detected AMPs concentrations of these months were not the lowest (Fig 2.4A). This may be because water vapor near the ground can strongly absorb the RAD_{LW} of ground[58], thus affecting the ES DFR_{LW}.

DRFs except for DRF_{LW} at ES were significantly negatively correlated with surface albedo (Spearman's correlation, $P<0.05$ for TOA DRF_{SW}, $P<0.01$ for TOA DRF_{LW} and ES DRF_{SW}, Fig 5.2). For aerosols that scatter the solar RAD_{SW}, more positive DRF_{SW} will be obtained with the increase of surface albedo[59]. For airborne materials that can absorb RAD_{LW} of ground, such as greenhouse gases, the DRF_{LW} will be more negative under higher surface albedo[60]. MPs are efficient at scattering RAD_{SW} and absorbing RAD_{LW}[19]. Therefore, the lowest DFR_{SW} at TOA (-0.03 W/m^2, Fig 5.1A), the second-to-last lowest DRF_{LW} at TOA (0.06 W/m^2, Fig 5.1A) and DFR_{SW} at ES (-0.15

W/m^2, Fig 5.1B) in Tianjin were all observed in November, which showed the highest surface albedo (0.213, Table 5.1). Ozone can absorb both of RAD_{SW} and RAD_L [61]. However, there was no significant correlation (Spearman's correlation, P>0.05) between AMPs DRFs and columnar ozone presented, indicating that ozone has a limited effect on AMPs DRFs.

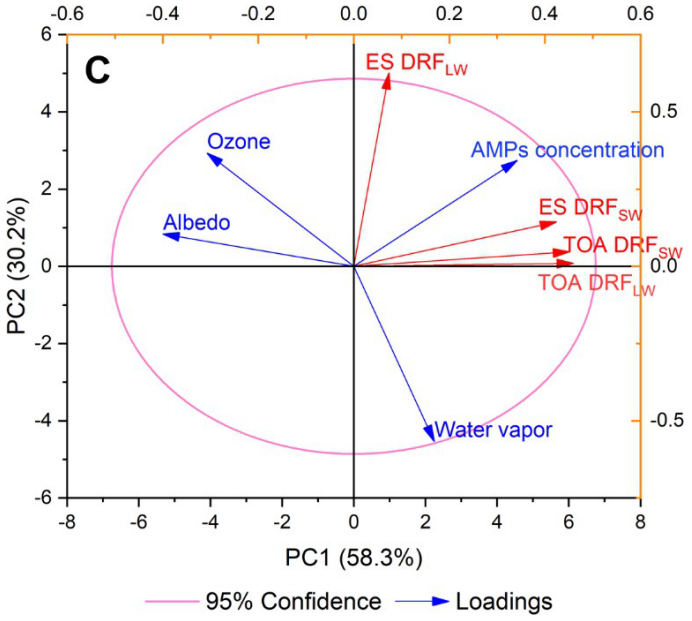

Figure 5.2 Monthly variation of shortwave DRF, longwave DRF, and net DRF at TOA (A) and ES (B), respectively. Principal component analysis (PCA) biplot of monthly AMPs DRFs and AMPs concentration as well as the environmental parameters (column ozone, water vapor, and surface albedo, Table 5.1).

5.3 AMPs DRF under different surface albedo.

To further describe the effect of surface albedo on the DRF of AMPs, the DRFs calculated based on two AMPs concentrations (200 and 600 n/m^3) as a function of the surface albedo at a range of 0.13 to 0.73, were provided (Fig 5.3). The concentrations of 200 and 600 n/m^3 represent the highest and lowest monthly AMPs concentration level in Tianjin, respectively. While the surface albedo of 0.13 and 0.73 represent the lowest surface albedo during sampling time (October) and the surface albedo on November when the ground was covered in snow (Table 5.4). In contrast to the linear relationship observed between DRF_{LW} and surface albedo, the relationship between DRF_{SW} and surface albedo did not demonstrate a linear trend (Fig 5.3A to D). As the surface albedo increases, the RAD_{SW} reflected by the ground increases. The repeated reflection of RAD_{SW} between the surface and AMPs leads to an extra absorption of RAD_{SW} by

atmospheric gases and surface, which can be described as a polynomial function related to the surface albedo[62]. The AMPs concentration near the ground surface is higher, thus compare to DRF_{SW} at TOA (Fig 5.3A and B), greater fluctuations in DRF_{SW} at ES (Fig 5.3C and D) with changes of surface albedo were observed. Overall, the concentration of AMPs affects the magnitudes of net DRF, but does not affect the direction of it (Fig 5.3A to D). Positive net DRF at ES were observed at all different surface albedos (Fig 5.3C and D). While the net DRF of AMPs at TOA became increasingly positive in the surface albedo range of 0.13 to 0.43 (Fig 5.3A and B), while decreased at surface albedo of 0.53 compared to that at 0.43, although the net DRF was still positive. And when the surface albedo was 0.73, the net DRF at TOA became negative again (Fig 5.3A and 3).

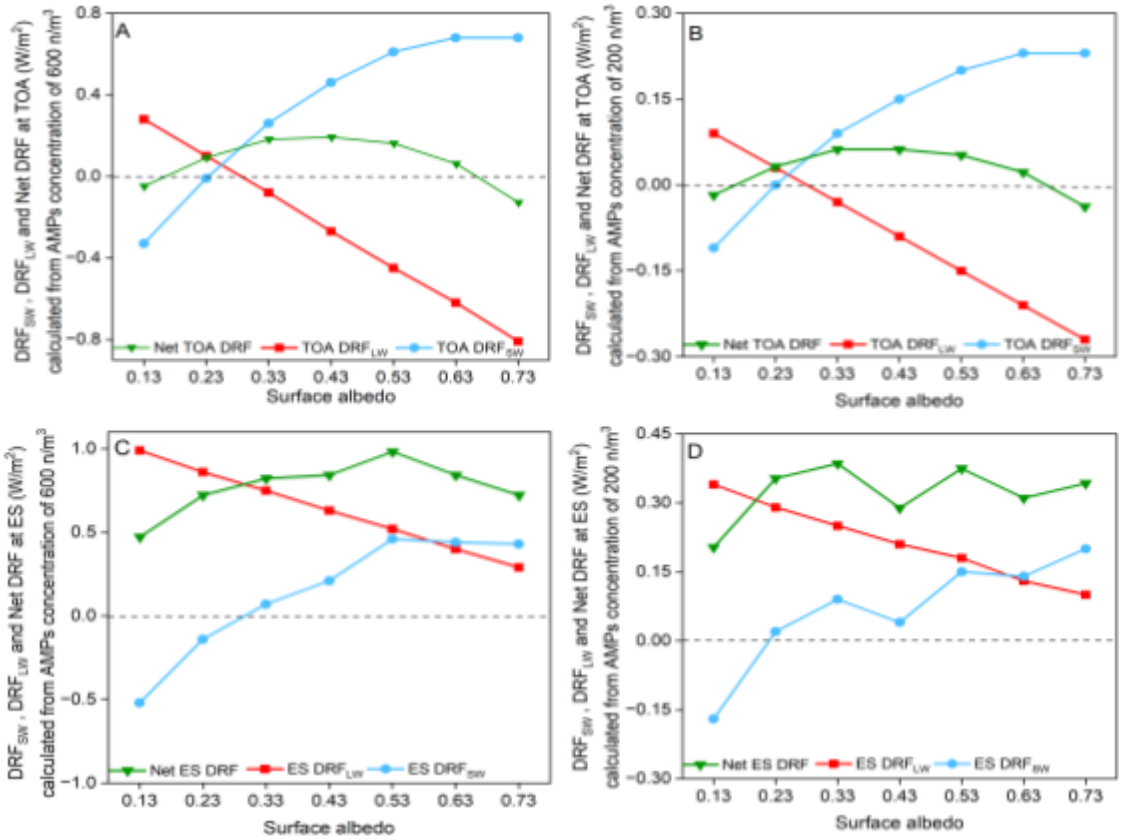

Figure 5.3 The calculated DRFs at TOA (A&B) and ES (C&D) as a function of surface albedos, based on AMPs concentrations of 600 n/m^3 (A&C) and 200 n/m^3 (B&D), respectively. The ozone and water vapor used in calculation were shown in Table 5.1.

Table 5.4 Snowfall amount of Tianjin during September 2021 to August 2022

Month	Nov	Dec	Jan	Feb	Mar
Snowfall (mm)	27.11	0.27	5.78	5.50	4.81

[a] Snowfall for months not listed in the table is 0.

The variation of the net DRF at TOA at different surface albedos was -0.09 to 0.13 W/m^2 (Fig 5.3A and B). For regions with a surface albedo of ~0.1, such as ocean[63] and forest land[64], the net DRF at TOA is expected to be negative (Fig 5.3A and B). For regions with a surface albedo of ~0.15, such as urban and crop land areas[64], the net DRF at TOA may be very small since DRF_{LW} and DRF_{SW} almost cancel each other out (Fig 5.3A and B). In grass and bare soil lands, net DRF at TOA tend to be positive because of the relative high surface albedo (approximately 0.2 to 0.23[64, 65]. For regions covered by snow and ice, which show the highest surface albedo (approximately 0.8)[66], the net DRF of AMPs at TOA is more likely to be negative (Fig 5.3A and 2B). Net DRF at TOA represents the disturbance of aerosol to the radiative balance of the earth-atmosphere system. Thus, net DRF at TOA can be used to evaluate the climate change caused by AMPs. That is, a positive net DRF at TOA indicates climate warming, while a negative net DRF indicates climate cooling. Considering that oceans account for approximately 70% of the Earth's surface, AMPs are expected to cause climate cooling in most of regions on the planet (Fig 5.4). For terrestrial environments, regions of grasslands and bare soil, where AMPs are prone to cause climate warming (Fig 5.4), account for 43% of the total land area (Table 5.4). In comparison, regions of forest and land covered by snow and ice, where AMPs are prone to cause climate cooling (Fig 5.4), account for 39% of the total land area (Table 5.5).

Table 5.5 Proportion of different land cover types on the Earth's surface[a] and the corresponding surface albedos.

Land cover types	Urban	Snow and ice	Bare soil	Crop land	Forest	Grass land
Land cover percentage (%)	0.2	9.7	13.3	15.7	29.4	30
Surface albedo	0.16	0.8	0.23	0.15	0.11	0.20

[a]Data of land cover types were derived from the World Agriculture and Food Organization (https://data.apps.fao.org/).

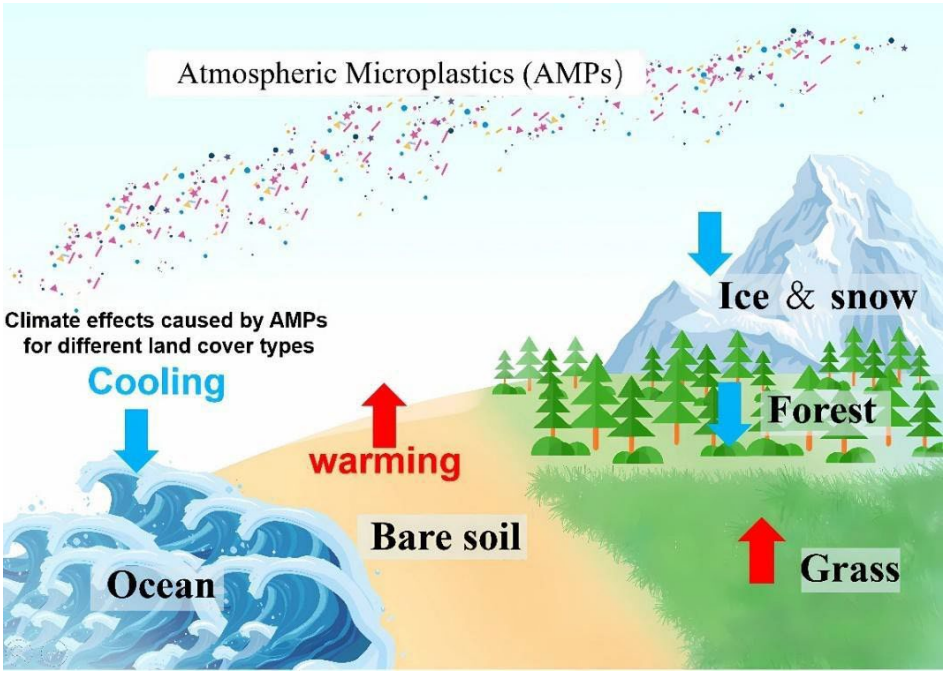

Figure 5.4 The calculated DRFs at TOA (A&B) and ES (C&D) as a function of surface albedos, based on AMPs concentrations of 600 n/m^3 (A&C) and 200 n/m^3 (B&D), respectively.

5.3 Climate effects caused by AMPs in different East Asian cities

Based on the observed atmospheric microplastic concentrations in the first half of 2022 (Fig 2.4A), the radiative forcings of three typical cities in East Asian were calculated. The average AMPs concentration of Mandalgobi, Tianjin and Toyama was 334.5±87.8 n/m^3, 215.1±49.7 n/m^3, and 156.8±23.0 n/m3 (Fig 5.5A), respectively, with the average net DRF at TOA as -0.005±0.013 W/m^2, 0.013±0.029 W/m^2 and 0.022±0.006 W/m^2 , respectively (Figure 5.5A). Although the AMPs concentration of Mandalgobi was significantly lower than that of the other cities (p<0.05), the absolute value of the average net DRF of AMPs at TOA was the highest. Due to the highest surface albedo, the DRF of AMPs in Mandalgobi was positive all the time (Fig 5.5B), thus resulting in a warming effect to the climate. The AMPs concentration of Toyama was significantly lower than that of Tianjin (Fig 5.5A), but the surface albedos of Toyama in most months during the first half of 2022 were relative high due to snowfall on the ground from January to April (Table 5.4), thus resulting in continuous positive net AMPs DRFs at TOA (Fig 5.5B). The surface albedo of Tianjin exhibited small fluctuations (0.151−0.198, Table 5.1), and as a result, the net DRF of AMPS at TOA also showed minor changes around zero (-0.02−0.01 W/m^2, Fig 5.5B). Therefore, the climate effect caused by AMPs of Tianjin was the weakest in threes targeted cities, although Tianjin showed the highest AMPs concentration during the first half of 2022.

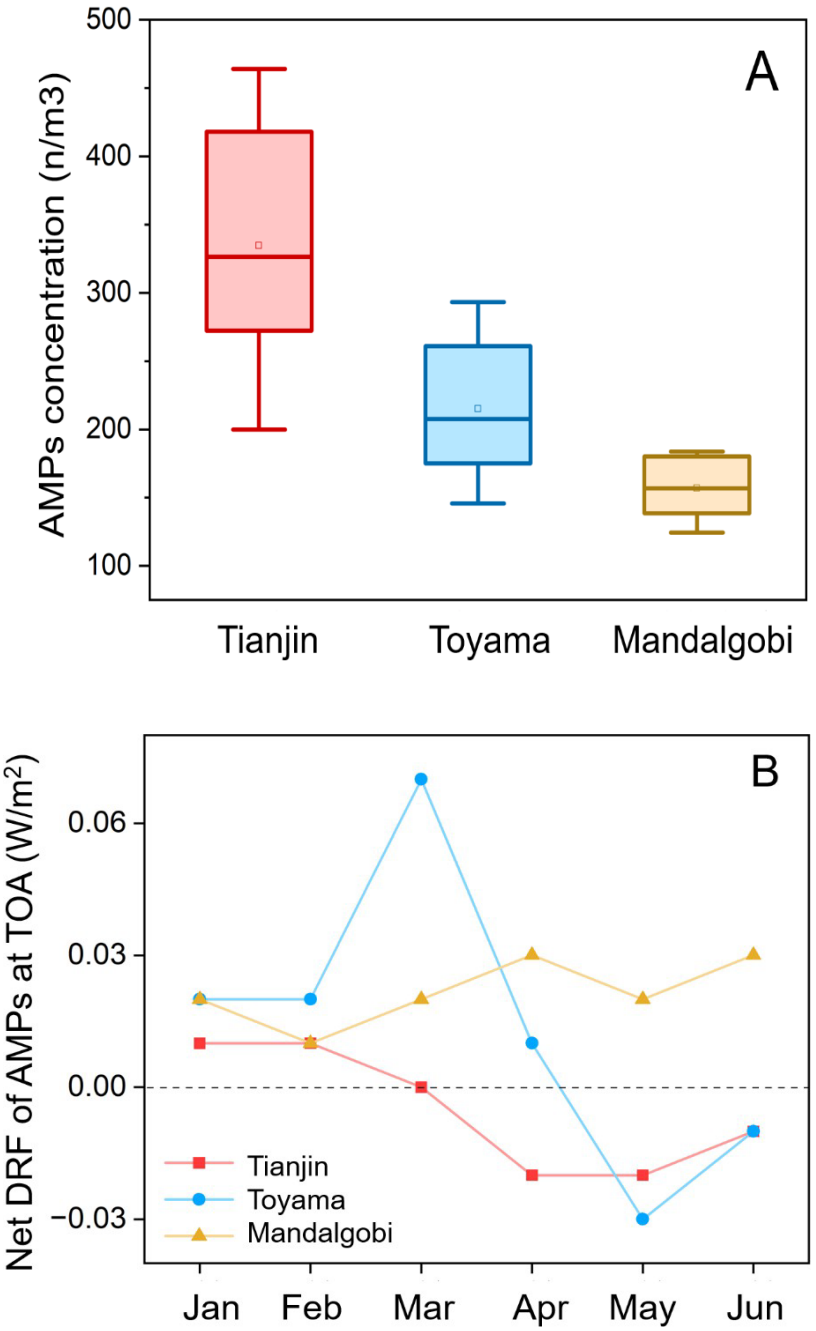

Figure 5.5 Concentrations of AMPs of Mandalgobi Tianjin and Toyama during the first half of 2022 (A). Monthly The net DRFs of AMPs of Mandalgobi, Tianjin and Toyama during the first half of 2022(B)

Table 5.4 Snowfall of Toyama and Mandalgobi during January 2022 to August 2022.

Month	1	2	3	4
Snowfall of Toyama (mm)	27.11	0.27	5.78	5.50

Snowfall of Mandalgobi（mm）	3.50	7.88	4.21

[a] Snowfall for months not listed in the table is 0.

Reference

1. Mu, J.L., et al., *Abundance and distribution of microplastics in the surface sediments from the northern Bering and Chukchi Seas.* ENVIRONMENTAL POLLUTION, 2019. **245**: p. 122-130.
2. Bergmann, M., et al., *White and wonderful? Microplastics prevail in snow from the Alps to the Arctic.* 2019. **5**(8): p. eaax1157.
3. Wright, S.L., et al., *Atmospheric microplastic deposition in an urban environment and an evaluation of transport.* ENVIRONMENT INTERNATIONAL, 2020. **136**.
4. Su, L., et al., *Using the Asian clam as an indicator of microplastic pollution in freshwater ecosystems.* ENVIRONMENTAL POLLUTION, 2018. **234**: p. 347-355.
5. Yuan, Z., et al., *Atmospheric microplastics at a southern China metropolis: Occurrence, deposition flux, exposure risk and washout effect of rainfall.* Science of The Total Environment, 2023. **869**: p. 161839.
6. Zhang, K., et al., *Microplastic pollution of lakeshore sediments from remote lakes in Tibet plateau, China.* ENVIRONMENTAL POLLUTION, 2016. **219**: p. 450-455.
7. Allen, S., et al., *Atmospheric transport and deposition of microplastics in a remote mountain catchment.* 2019.
8. Brahney, J., et al., *Plastic rain in protected areas of the United States.* 2020. **368**(6496): p. 1257-1260.
9. Dong, H., et al., *Microplastics in a Remote Lake Basin of the Tibetan Plateau: Impacts of Atmospheric Transport and Glacial Melting.* Environmental Science & Technology, 2021. **55**(19): p. 12951-12960.
10. Chen, Q., et al., *Long-range atmospheric transport of microplastics across the southern hemisphere.* Nature Communications, 2023. **14**(1): p. 7898.
11. Qian, Z.A., et al., *Some Advances in Dust Storm Researches in Northern China.* 2004.
12. Chung, Y.S., H.-S. Kim, and Y. Chun, *On large-scale transport of dust storms and anthropogenic dust-falls over east Asia observed in central Korea in 2009.* Asia-Pacific Journal of Atmospheric Sciences, 2014. **50**(3): p. 345-354.
13. Lee, E.H. and B.J. Sohn, *Recent increasing trend in dust frequency over Mongolia and Inner Mongolia regions and its association with climate and surface condition change.* ATMOSPHERIC ENVIRONMENT, 2011. **45**(27): p. 4611-4616.
14. Xu, L., et al., *Tracing the evolution of morphology and mixing state of soot particles along with the movement of an Asian dust storm.* 2020.
15. Sultanova, N.G., S.N. Kasarova, and I.D.J.A.P.P.A. Nikolov, *Dispersion Properties of Optical Polymers.* 2009(4).
16. Loewenstein, E.V. and D.R. Smith, *OPTICAL CONSTANTS OF FAR INFRARED MATERIALS-1.* 1971.
17. Zhang, X., et al., *Complex refractive indices measurements of polymers in visible and near-infrared bands.* **59**(8): p. 2337-2344.
18. A, X.Z., et al., *Complex refractive indices measurements of polymers in infrared bands - ScienceDirect.* **252**.
19. Revell, L.E., et al., *Direct radiative effects of airborne microplastics.* 2022. **598**(7881): p. 462-467.
20. Liu, C., et al., *Widespread distribution of PET and PC microplastics in dust in urban China and their estimated human exposure.* 2019. **128**.

21. Dris, R., et al., *A first overview of textile fibers, including microplastics, in indoor and outdoor environments.* Environmental Pollution, 2017. **221**: p. 453-458.
22. Levermore, J.M., et al., *Detection of Microplastics in Ambient Particulate Matter Using Raman Spectral Imaging and Chemometric Analysis.* Analytical Chemistry, 2020. **92**(13): p. 8732-8740.
23. Liu, K., et al., *Consistent Transport of Terrestrial Microplastics to the Ocean through Atmosphere.* Environmental Science & Technology, 2019. **53**(18).
24. Chang, D.Y., et al., *First quantification and chemical characterization of atmospheric microplastics observed in Seoul, South Korea.* Environmental Pollution, 2023. **327**: p. 121481.
25. Klein, M. and E.K. Fischer, *Microplastic abundance in atmospheric deposition within the Metropolitan area of Hamburg, Germany.* Science of The Total Environment, 2019. **685**: p. 96-103.
26. Tian, Y.J., et al., *An innovative evaluation method based on polymer mass detection to evaluate the contribution of microfibers from laundry process to municipal wastewater.* JOURNAL OF HAZARDOUS MATERIALS, 2021. **407**.
27. Ayankunle, A.Y., et al., *Estimating Microplastics related to Laundry Wash and Personal Care Products released to Wastewater in Major Estonian Cities: a comparison of calculated and measured microplastics.* JOURNAL OF ENVIRONMENTAL HEALTH SCIENCE AND ENGINEERING, 2023. **21**(1): p. 225-237.
28. Borthakur, A., et al., *Inhalation risks of wind-blown dust from biosolid-applied agricultural lands: Are they enriched with microplastics and PFAS?* Current Opinion in Environmental Science & Health, 2022. **25**: p. 100309-Article No.: 100309.
29. Long, Z.X., et al., *Heterogeneity and Contribution of Microplastics From Industrial and Domestic Sources in a Wastewater Treatment Plant in Xiamen, China.* FRONTIERS IN ENVIRONMENTAL SCIENCE, 2021. **9**.
30. Cui, Y.F., et al., *Effects of Urban Surface Roughness on Potential Sources of Microplastics in the Atmospheric Boundary Layer.* BOUNDARY-LAYER METEOROLOGY, 2023. **186**(3): p. 425-453.
31. Tian, X., et al., *Amount and characteristics of microplastic and organic matter in wind-blown sediment at different heights within the aeolian sand saltation layer.* ENVIRONMENTAL POLLUTION, 2023. **327**.
32. Brahney, J., *<PNAS constrain ATMOS cycle.pdf>*. PNAS, 2021.
33. Isari, E.A., et al., *Microplastics in Agricultural Soils: A Case Study in Cultivation of Watermelons and Canning Tomatoes.* WATER, 2021. **13**(16).
34. Yang, Z., et al., *A neglected transport of plastic debris to cities from farmland in remote arid regions.* SCIENCE OF THE TOTAL ENVIRONMENT, 2022. **807**.
35. Kai, et al., *Source and potential risk assessment of suspended atmospheric microplastics in Shanghai.* 2019.
36. Szewc, K., B. Graca, and A. Dołęga, *Atmospheric deposition of microplastics in the coastal zone: Characteristics and relationship with meteorological factors.* Science of The Total Environment, 2020: p. 143272.
37. Wang, X., et al., *Efficient transport of atmospheric microplastics onto the continent via the East Asian summer monsoon.* Journal of Hazardous Materials, 2021. **414**: p. 125477.
38. Leonard, J., et al., *The relative importance of local climate and land use on the deposition rate of airborne microplastics on terrestrial land.* Atmospheric Environment, 2024. **318**: p. 120212.
39. *Junjie Zhang*, et al.,*Quantitative evaluation of non-active land input of microplastics: Acase pf PET polymer,2021,66(13):1563-1570.*
40. Wang, T., et al., *Preliminary study of the source apportionment and diversity of*

microplastics: Taking floating microplastics in the South China Sea as an example. Environmental Pollution, 2019. **245**: p. 965-974.
41. Ballent, A., et al., *Sources and sinks of microplastics in Canadian Lake Ontario nearshore, tributary and beach sediments.* Marine Pollution Bulletin, 2016. **110**(1): p. 383-395.
42. Peng, C., et al., *Source apportionment of microplastics in indoor dust: Two strategies based on shape and composition.* ENVIRONMENTAL POLLUTION, 2023. **334**.
43. Yang, Z., M. Çelik, and H. Arakawa, *Challenges of Raman spectra to estimate carbonyl index of microplastics: A case study with environmental samples from sea surface.* Marine Pollution Bulletin, 2023. **194**: p. 115362.
44. Zhang, Y., et al., *Comparison of Detection Methods of Microplastics in Landfill Mineralized Refuse and Selection of Degradation Degree Indexes.* Environmental Science & Technology, 2021. **55**(20): p. 13802-13811.
45. Hee, Y.Y., et al., *Atmospheric microplastic transport and deposition to urban and pristine tropical locations in Southeast Asia.* Science of The Total Environment, 2023. **902**: p. 166153.
46. Wang, Y.Q., *MeteoInfo: GIS software for meteorological data visualization and analysis.* METEOROLOGICAL APPLICATIONS, 2014. **21**(2): p. 360-368.
47. Chunguang, et al., *Widespread distribution of PET and PC microplastics in dust in urban China and their estimated human exposure.* 2019.
48. Chen, Y., et al., *Wet Deposition of Globally Transportable Microplastics (<25 μm) Hovering over the Megacity of Beijing.* Environmental Science & Technology, 2023. **57**(30): p. 11152-11162.
49. Huang, Y., et al., *Atmospheric transport and deposition of microplastics in a subtropical urban environment.* 2021. **416**(4): p. 126168.
50. Ricchiazzi, et al., *SBDART: A Research and Teaching Software Tool for Plane-Parallel Radiative Transfer in the.* 1998.
51. Henze, D.K., et al., *Spatially Refined Aerosol Direct Radiative Forcing Efficiencies.* Environmental Science & Technology, 2012. **46**(17): p. 9511-9518.
52. Shamjad, P.M., et al., *Contribution of Brown Carbon to Direct Radiative Forcing over the Indo-Gangetic Plain.* Environmental Science & Technology, 2015. **49**(17): p. 10474-10481.
53. Shamjad, P.M., et al., *Absorbing Refractive Index and Direct Radiative Forcing of Atmospheric Brown Carbon over Gangetic Plain.* ACS Earth and Space Chemistry, 2018. **2**(1): p. 31-37.
54. Bibi, S., et al., *Observations of black carbon aerosols characteristics over an urban environment: Radiative forcing and related implications.* Science of The Total Environment, 2017. **603-604**: p. 319-329.
55. Yuan, Q., et al., *Evidence for Large Amounts of Brown Carbonaceous Tarballs in the Himalayan Atmosphere.* 2020.
56. Hess, M., P. Koepke, and I.J.B.o.t.A.M.S. Schult, *Optical properties of Aerosols and Clouds: The Software Package OPAC.* 1998. **79**(5): p. 831-844.
57. Dessler, A.E., et al., *An analysis of the dependence of clear-sky top-of-atmosphere outgoing longwave radiation on atmospheric temperature and water vapor.* 2008. **113**(D17): p. -.
58. Ramanathan, V. and J.A.J.R.o.G. Coakley, *Climate modeling through radiative - convective models.* 1978. **16**(4).
59. Boucher, O. and T.L.J.J.o.G.R.A. Anderson, *General circulation model assessment of the sensitivity of direct climate forcing by anthropogenic sulfate aerosols to aerosol size and chemistry.* 1995. **100**(D12).
60. Menon, S., et al., *Radiative forcing and temperature response to changes in urban*

albedos and associated CO₂ offsets. ENVIRONMENTAL RESEARCH LETTERS, 2010. **5**(1).
61. Myhre, G., et al., *Radiative forcing due to changes in tropospheric ozone in the period 1980 to 1996.* 2000. **105**(D23): p. 28935-28942.
62. J. M. Haywood, K.P.S., *Multi - spectral calculations of the direct radiative forcing of tropospheric sulphate and soot aerosols using a column model.* Q.J.R. Meteorol. Soc., 1997. **123: 1907-1930**.
63. Qu, Y., *5.07 - Sea Surface Albedo*, in *Comprehensive Remote Sensing*, S. Liang, Editor. 2018, Elsevier: Oxford. p. 163-185.
64. *Intra-annual variability of satellite observed surface albedo associated with typical land cover types in China %J Journal of Geographical Sciences.* 2015. **01**(v.25): p. 37-46.
65. Yang, F. and J. Zhou. *Measurement of surface albedo and its environmental effects over a temperate desert steppe*. in *International Conference on Photonics & Image in Agriculture Engineering*.
66. Kokhanovsky, A.A., *The Broadband Albedo of Snow.* FRONTIERS IN ENVIRONMENTAL SCIENCE, 2021. **9**.